SAND79-1855
Unlimited Release

Final Report: Conasauga Near-Surface Heater Experiment

James L. Krumhansl

Sandia Laboratories

3900 Q(7-73)

SAND79-1855
Unlimited Release
Printed November 1979

FINAL REPORT: CONASAUGA NEAR-SURFACE HEATER EXPERIMENT

James L. Krumhansl
Geological Projects Division 4537
Sandia Laboratories
Albuquerque, New Mexico 87185

ABSTRACT

The Conasauga Experiment was undertaken to begin assessment of the thermomechanical and chemical response of a specific shale to the heat resulting from emplacement of high-level nuclear wastes. Canister-size heaters were implanted in Conasauga shale in Tennessee. Instrumentation arrays were placed at various depths in drill holes around each heater. The heaters operated for 8 months and, after the first 4 days, were maintained at 385°C. Emphasis was on characterizing the thermal and mechanical response of the formation. Conduction was the major mode of heat transport; convection was perceptible only at temperatures above the boiling point of water. Despite dehydration of the shale at higher temperatures, in situ thermal conductivity was essentially constant and not a function of temperature. The mechanical response of the formation was a slight overall expansion, apparently resulting in a general decrease in permeability. Metallurgical observations were made, the stability of a borosilicate glass wasteform simulant was assessed, and changes in formation mineralogy and groundwater composition were documented. In each of these areas, transient nonequilibrium processes occur that affect material stability and may be important in determining the integrity of a repository. In general, data from the test reflect favorably on the use of shale as a disposal medium for nuclear waste.

ACKNOWLEDGMENTS

The author gratefully acknowledges the contributions of many individuals. Specia recognition is due to the following Sandia Laboratories personnel for their efforts:

E. A. Ames	Design and installation of transducers (thermocouples, stress gauges, extensometers, *pressure gauges*)
A. J. Anaya	Thermal conductivity and thermal expansion measurements on core samples
A. C. Arthur	Mechanical design
J. W. Braithwaite	Metallurgical experiment
S. L. Brandon	Manuscript preparation
F. J. Conrad	Gas analysis
R. L. Courtney	Thermal expansion, heat capacity, SEM, DTA, TGA, specific surface area, and grain density laboratory measurements on core samples
C. O. Duimst.a	Instrumentation project engineer
S. L. Erickson	Water sample analysis
J. L. Golden	Water sample analysis
D. M. Heinze	X-ray analysis of core samples
R. D. Klett	Transmissivity modeling
J. T. Lindman	Instrument van operation
D. F. McVey	Thermal modeling
P. L. Mead	Manuscript preparation
C. D. Northam	*Transmissivity*
P. J. Rodacy	Gas analysis
M. A. Stark	Core processing, sample preparation, and photomicrographs
W. D. Sundberg	Thermal modeling
J. R. Tillerson	*Mechanical modeling*
W. Wawarsik	Rock mechanics laboratory measurements
W. C. Wilson	Construction project engineer and transmissivity measurements
S. F. Yager	Wattmeter design

The site support provided by Dow Odum and Luther Lavell of the Oak Ridge National Laboratory Plant Engineering Department during experiment construction and operation contributed greatly to the project's efficiency.

CONTENTS

ILLUSTRATIONS

ILLUSTRATIONS (Continued)

ILLUSTRATIONS (Continued)

TABLES

FINAL REPORT: CONASAUGA NEAR-SURFACE HEATER EXPERIMENT

I. INTRODUCTION

The Conasauga Near-Surface Heater Experiment was undertaken to determine whether a specific shale would respond favorably to the thermal loading that would accompany emplacement of a high-level nuclear waste canister. The principal objectives of the test were to measure what changes, if any, occurred in in situ thermal conductivity as a consequence of heating, to assess whether conduction or convection was the primary mechanism of heat transfer, and to note whether the mechanical response of the formation resulted in a significant change in rock mass permeability. Beyond allowing for studying the thermal and mechanical responses of the rock, however, the test also provided an opportunity to investigate other processes pertinent to the design of a repository or a vault test at depth. Mineralogic changes were noted as well as variations in groundwater composition. Corrosion characteristics of a variety of potential canister materials were also noted. Finally, a sample of borosilicate glass nuclear waste simulant was included so that its stability in such an environment could be assessed.

Near-surface in situ heater tests serve as a bridge between the idealized concepts that dictate the course of laboratory and modeling programs and the response to be expected under actual repository conditions where all the complexities of nature operate simultaneously. Such tests are done on a scale large enough to allow measurement of the properties of rock assemblages rather than the behavior of the smaller samples characteristic of laboratory experiments. The near-surface environment also provides a place to test whether models under development can accurately predict the responses of a particular assemblage of rock types. Finally, such tests provide insight into whether laboratory and modeling programs are directed toward issues that will ultimately be critical to the integrity of an actual repository. Once there is a thorough understanding of phenomena observed during near-surface tests, it should be possible to properly design more elaborate and costly at-depth vault tests to demonstrate the viability of a particular disposal concept. It should be emphasized, however, that a near-surface test in itself cannot answer all the complex questions pertinent to a particular disposal concept or provide for full model validation.

Briefly, the Conasauga Near-Surface Heater Experiment consisted of two canister-size heaters (0.3 metre in diameter and 3 metres in length) implanted at depths of about 15 metres in the Conasauga Shale (Figure 1).* The heaters were placed in holes S1-1 and S2-1 at Sites 1 and 2, respectively (Figure 2), with

*All figures follow the text.

thermocouples, vertical extensometers, and horizontal stress gauges placed in arrays of drill holes surrounding the heaters. The heaters were turned on at Sites 1 and 2 on 29 November and 6 December 1977, respectively. Following a startup phase which lasted 4 days, the heaters were operated with a midplane temperature of 385°C for 239 days (Site 1) and 232 days (Site 2). Details of the design and operation of the experiment are described in Sections III, IV, and V of Reference 1. After 150 days of operation, a preliminary data analysis was undertaken that resulted in the following tentative conclusions:

1. In situ thermal conductivities range from 1.5 to 2.0 W/m°C,
2. In situ thermal conductivities do not drop precipitously at temperatures above 100°C, despite the marked reduction noted when unconfined shale samples become dried during laboratory tests,
3. Heat transfer in the formation is dominated by conduction, although a perceptible displacement of isotherms is caused by convecting steam in the region immediately around the top of the heater,
4. Through-flowing groundwater has not transported a detectable amount of energy away from the heater locations,
5. The overall in situ behavior of the formation is a modest thermal expansion, despite the contraction commonly observed in the laboratory, and
6. Water loss and the presence of even moderate amounts of confining pressure influence the behavior of shale to the extent that control of these variables in the laboratory must adequately duplicate the field situation, or the parameters determined will be of little use in modeling field-test results.

Subsequent data and analyses discussed below support these conclusions.

The report is divided into three sections. The first documents the concluding months of the field experiment. The second presents a final synthesis of field and laboratory data. The third is a discussion of the field test as it pertains to the disposal of high-level waste (HLW). For additional details regarding the experiment design and goals, the reader is referred to the preliminary results report.[1]

II. FIELD ACTIVITIES

From the time of preliminary data assessment until test completion, three phases of field activities were carried out. The heaters operated in essentially a steady-state mode from April through July 1978. Heater power was turned off on 1 August, and the thermal decay of the sites was monitored for an additional 2 months. Beginning 1 October 1978, the heaters were recovered and the sites decommissioned.

Continued Heater Operation (April-July 1978)

The steady-state operation of the heaters from April through July 1978 was an extension of the operating conditions that had persisted since roughly February 1978. Prior to this time, both isotherm positions [Figures 3(a) and (b)] and heater wattages [Figure 3(c)] changed rapidly to accommodate a fixed heater temperature that was established in the first week of operation. During the last months of operation, no significant changes were noted in the formation's thermal behavior. At Site 1, isotherms parallel and perpendicular to strike were virtually identical (Figure 4). At Site 2, however, the thermocouple string at a radius of 0.6 metre perpendicular to strike consistently read 5 to 10 degrees above measurements made at analogous positions parallel to strike. This asymmetry may reflect either the up-dip migration of steam or a genuine asymmetry in the formation's thermal conductivity.

Within the detection capabilities of the operating instrumentation, major changes in mechanical response of the formation were also absent during this period. Early in the test, extensometers changed relative positions rapidly, but during the last 4 months, no perceptible changes occurred. That the airflow required to maintain pressure in the heater holes remained essentially constant was further evidence precluding the possibility of gross fracturing of the formation during this latter period of the test. Thus, the essentially static isotherm positions occurred in a time period during which formation displacement also was minimal. It follows that, in these tests, the value of prolonged experimentation lay in assessing the long-term effects that essentially static conditions had on material properties rather than in gaining information from the relatively small changes in mechanical or thermal response which occurred during the later stages of the test.

Cooldown (August-September 1978)

Before the power was turned off, particular care was taken to establish baseline data regarding site hydrology and airflow required to keep groundwater

from the sites. In addition, water samples were taken before and during cooldown for chemical analyses. To simplify interpretation of cooling rates and to prevent flooding of the heaters, air pressure was maintained on the heater holes until the day of heater recovery.

On 1 August at 1330, power to both sites was turned off. The maximum temperature at either site before turnoff was 400°C at Site 2 (Figure 4). After 8 days, the maximum temperature at both sites had dropped below 100°C. No quenching effects due to groundwater influx were noted during this period. Airflow required to maintain preset air pressures in the Site 1 heater hole showed only a slight increase after heater turnoff (Figure 5). This response may have been due to the absence of steam or to minor contraction and cracking of the formation. At Site 2, a relatively permeable fracture zone in the heater hole at a depth of between 10 and 12 metres required a substantially higher airflow (8.5×10^{-2} m^3/min) to prevent flooding during the test. Consequently, the relatively small changes induced by cooling could not be detected. Minor fluctuations in water level in satellite wells occurred during this period; however, they could not be related to the cooling process (Figure 6). In conclusion, only minor changes occurred within the shale as a consequence of cooling of the formation.

Decommissioning and Post-Test Activities (September-December 1978)

Decommissioning of the sites, which extended from October through December 1978, was subject to two constraints. A prescribed sequence for post-test activities was necessary so that post-test in situ analysis was not jeopardized and so that the operation could be completed before winter. Because of the first constraint, decommissioning activities were scheduled in the following order:

1. Heater recovery and downhole photographic documentation,
2. Post-test transmissivity measurements, and
3. Post-test core drilling.

1. Recovery of Heaters and Downhole Photographic Documentation

The heater at Site 2 was easily recovered despite a bend in the hole at a depth of about 14 metres. At Site 1, the heater initially seemed to be wedged in the hole, and the recovery effort was postponed until the next day. The heater was then recovered with very little effort but with a substantial boot of scale adhering to its bottom. Presumably, as a result of leaving air pressure off the hole overnight, enough water entered the hole to loosen the scale and float the heater free.

After both heaters had been recovered, it became evident that the air pressure applied to exclude groundwater had caused rather different conditions to exist in the two heater holes. The pressure applied to Site 2 (0.19 MPa) had been presumed to be sufficient to virtually exclude water from the heater hole throughout the test. In fact, the only signs of water entering during the test were a white stain down the side of the heater and a water mark roughly 10 to 15 cm

from the heater bottom (Figure 7). Parenthetically, from this water mark, it appears that the heater was inclined at an angle of roughly 5° from the vertical. Over most of its surface, the heater showed a reddish bronze discoloration indicative of a thin uniform oxide coating.

The pressure applied at Site 1 (0.08 MPa) was not sufficient to keep water from the site. During much of the test, there must have been a small amount of standing water in the bottom of the heater hole. In contrast to Site 2, the high-water mark on this heater was about 0.6 metre from the heater bottom (Figure 8). Scale deposited over the bottom 0.25 metre of the heater was up to 2.5 cm thick and consisted of roughly equal parts of shale fragments and anhydrite cement. Farther up the heater, scale thickness was generally less than 0.5 cm. The banded appearance in this interval, as well as the presence of numerous recemented scale fragments in the scale coating, suggest that water repeatedly advanced and retreated, often quenching the heater as it progressed.

In addition to precipitating a substantial amount of material from solution, water boiling in the heater hole at Site 1 greatly increased corrosion rates above the water level. Unlike Site 2, the surface of the Site 1 heater had numerous small areas where corrosion was somewhat intensified, though it had not progressed to the extent that it was a threat to the heater shell. Localized corrosion on the heater was most common in the vicinity of the high-water mark and on the top 0.6 metre of the heater, which contained the junction section and which consequently was relatively cool. The external thermocouples at the top of the heater were also severely corroded. In contrast, beneath the scale, the heater retained a silvery metallic appearance and showed little evidence of corrosion. For additional details, refer to later sections that deal specifically with mineralogy and metallurgy.

The recovered heaters were shipped to the Nevada Test Site and disassembled for inspection. The general internal condition of both heaters was considered to be excellent. The following observations were made:[2]

a. Element resistance had increased by 9 to 13%. The reason for this change is unknown.

b. Surface rust spots showed on the Inconel element sheath on Heater 1; however, visual inspection revealed no perceptible attack on the metal. When the spots were scraped, bright Inconel showed underneath. Heater 2 had no such spots on the elements.

c. There had been moisture leakage through the junction section header into the vermiculite-filled cold section on both heaters (Heater 1 more than Heater 2). This moisture leakage occurred in two areas; one at the vermiculite fill cover and the other around each element where an asbestos washer was used for the compressive element feedthrough. Elimination of the washer and welding of the feedthroughs would solve the second leakage problem, but a different design should be worked out for the vermiculite fill cover.

d. Water had been standing in the junction section for long periods of time in both heaters, as shown by rust marks in these areas. Heater 1 apparently

had about 2.5 cm of standing water and Heater 2 had about 1.25 cm. It is believed that this water was probably from the exhaust fan system which keeps the junction section cool. As moisture-laden, warm, outside air is pulled to depth through the inlet pipe, it precipitates moisture on the cool steel pipe. These droplets then combine and run down into the junction section. The process must reach an equilibrium state since the water went no higher than 2.5 cm, even though there was an almost infinite supply of humid air.

Water accumulation in this section could have disastrous results in that the terminals in this area have not been purposely moisture-proofed, and complete water submersion could well result in electrical shorts either to the heater case, which is at ground potential (ΔEMF = 110 VAC), or to another of the active elements (ΔEMF = 208 VAC). The terminals were coated with an epoxy-like material to reduce oxidation, and this coating may have afforded some protection against arcing. Future application of this type of heater design should account for this potential problem and allow for water removal, and possibly hard-potting or some other method must be used to completely waterproof the terminals. Alternate methods of cooling the junction section should also be considered, as well as the feasibility of eliminating the requirements for cooling by complete redesign of the junction section.

e. Also found in the junction section was an accumulation of moths, spiders, mosquitoes, etc., all coated with reddish rust. Since all parts of the junction section are stainless steel, the rusty water must have come from higher up in the pipe string, where standard pipe was used. Fine mesh screen across the inlet would probably keep most of the insect-like creatures out, but it could easily be clogged by their bodies enough to decrease the airflow (and to require some operator maintenance).

f. The thermocouples (TCs) inside the heater, though discolored, seemed to be in excellent condition, with no hint of the corrosion seen on the outside TCs. All the external TCs on Heater 1 showed massive corrosion downward for a distance of 0.7 metre from the top of the heater [above the heated section and beneath the protective sheath), just as they did above the top of the heater. The Heater 2 external TCs were bright and shiny, with no hint of corrosion.

Immediately following heater recovery, the condition of the heater-hole walls was recorded on videotape using a downhole television camera. This was done to note the size, orientation, and location of any heat-induced fractures. Assuming a positive thermal expansion, the most probable location for fracturing would have been at the heater midplane. Shales, however, commonly show an initial thermal contraction in the laboratory, corresponding to water loss from the clay minerals. This is followed by a less pronounced positive thermal expansion as the dried material is heated further. Modeling this behavior indicated that, at a rapid heating rate, fracturing could have occurred immediately above or below the heater.

Photographs which were taken before and after the test and compared indicated a lack of new fractures in either of these localities [Figures 9(a) and (b), 10(a) and (b)]. Annular gouges made during the drilling operation were

evident over the entire length of both heater holes. Preservation of these features and an absence of large accumulations of shale fragments along the sides of or on top of the heaters also ruled out the possibility that substantial spalling occurred from the hole walls.

2. Post-Test Transmissivity Measurements

In addition to recording the condition of the hole walls photographically, techniques were employed to determine whether the bulk permeability of the formation changed significantly or whether substantial new fractures formed distally. Basically, air pressure was applied to an injection well (either the heater hole or one of the accessible instrumentation holes), and the flow both into the injection well and out of an exit well was recorded. Additional information was gained by releasing a ^{85}Kr tracer in the injection well and noting the arrival times on an array of Geiger-Muller tubes placed at various depths in the exit well. Under optimal conditions, this technique may yield quantitative estimates of changes in bulk permeability or fracture transmissivity. At this depth, however, the Conasauga formation is not the optimal setting for such determinations. Bedding is pronounced, and many of the bedding plane partings open to different degrees at various localities. Furthermore, complex interlocking networks of small cracks subdivide the formation into irregular domains of greater or lesser permeability that are of the same scale as the distances between drill holes in the formation. Thus, measurements of the type described above were necessarily averages over regions having substantially different qualities.

Although the Conasauga is far from a uniform porous medium, the following relationship has proven useful in normalizing data taken under somewhat different conditions before and after the test:[3]

$$\left(\frac{k}{e}\right) \propto \frac{S^2 \ln\left(\frac{2S}{r_0}\right)}{3\,\Delta P\, T_f}$$

where

k = hydraulic conductivity,

e = void fraction,

r_0 = radius of injection well,

S = half the distance between holes,

ΔP = pressure drop between holes, and

T_f = time of first arrival.

It is evident (Figure 11) that most of the data taken before the test cluster at higher values of k/e than do those taken after the test. The relative changes that occurred during the test are more relevant. Points joined by dashed lines in Figure 11 represent before/after comparisons made between the same pairs of injection and exit wells. In every case, the post-test value of k/e was less than observed before the test. The above discussion pertains primarily to flow in a porous medium. Between S1-1 and S1-3, there was one single, well-defined fracture, as indicated by the fact that tracer tests between these two holes

yielded peaks that grew and decayed in a matter of minutes, as contrasted with peaks lasting 1/2 hour or more in all other well combinations. In this one case with a well-defined fracture, travel times remained essentially unchanged, despite the fact that the driving pressure in the post-test measurement was twice that in the pretest determination. In other words, following the test, the decreased permeability characteristic of the bulk formation was matched by a decreased transmissivity along a well-defined fracture.

It may be inferred from the variation in k/e noted above either that the permeability of the formation generally decreased or that the amount of open void space in the formation increased relative to the condition before the heating cycle. It is possible to distinguish between these two possibilities by examining the steady-state airflow measurements made in conjunction with the transmissivity tests (Figures 12 and 13). Generally, the steady-state airflow from a hole varies inversely with permeability. Thus, it is immediately evident from the clustering of pre- and post-test data that a substantial permeability decrease occurred during the test. Another piece of evidence corroborates this contention. At Site 2, water failed to fill the heater hole for several weeks after air pressure had been removed. Before the test, however, the hole would commence filling at a rate of about 13 litres per hour as soon as air pressure was removed.

3. Post-Test Core Drilling

Another method of assessing the effects of the heating cycle was by direct sampling. Following cooldown, core samples were taken from both sites, primarily for mineralogical and textural analyses. From these cores, however, it was also possible to determine the extent to which the surrounding rock had been influenced by the applied air pressure. At Site 1, the pressure applied (0.08 MPa) was barely adequate to prevent inundation of the heater, and only subtle changes were discernible. In fact, even in cores that had been exposed to temperatures of 200°C for much of the test, the only discernible changes were a slight brownish discoloration of the shale and a loss of sheen on some slickensided shear surfaces. In a hole 0.6 metre from the center, the brownish discoloration disappeared at about the 100°C isotherm, implying that groundwater could retard shale oxidation. There was no evidence that mineralization had occurred on open fractures, that new fractures had formed, or that motion had occurred on old fractures.

The 0.19 MPa pressure applied to Site 2 resulted in virtually complete exclusion of groundwater and constituted a significant fraction of the lithostatic pressure just below the cased part of the heater hole. At Site 2, the bulk of the material behaved like that at Site 1. However, the greater air pressure caused hot air and steam to move outward along the numerous networks of preexisting fractures in the formation. Intensely oxidizing conditions existed along these fractures, resulting in a brick-red surface discoloration that generally did not extend more than 0.1 mm outward into the shale. At a radius of 1 metre, zones of intense oxidation were most common at depths between 13 and 18 metres

and occurred in regions where formation temperature ranged from 150°to 60°C. Coloration was absent in a drill hole 2.6 metres from the heater, although the peak temperature in this hole was about 60°C.

To summarize, on the basis of field evidence, it appears that the shale stood the heating cycle well, and fluid circulation was apparently of a restricted nature. No new fractures appear to have opened in the heater hole walls, nor did spalling from the wall occur to the extent that heater recovery was impaired. The same assessment apparently applies to the formation as a whole. Core drilling failed to produce any surprises, and the formation as a whole experienced decreased permeability apparently as a consequence of the compression experienced during heating. It follows, then, that the subtle changes that did occur as a result of heating are best documented by careful comparisons of field data with the results of laboratory and modeling programs.

III. MODELING AND LABORATORY ACTIVITIES

Thermal Modeling

Much of the information regarding the thermal response of the Conasauga Experiment has already been reported;[1] but briefly, the principal findings were that in situ conductivity on the whole was between 1.5 and 2.0 W/m°C, that no precipitous drop in conductivity occurred in the volume between the heater and the 100°C isotherm, and that convection played a small but perceptible part in heat dissipation within the 100°C isotherm. To gain a better understanding of the in situ conduction process, a parametric study (with the computer code CINDA)[4] was undertaken using various temperature-independent thermal conductivities between 1.5 W/m°C and 2.25 W/m°C. In addition, the effects of a temperature-dependent thermal conductivity were assessed by using two pairs of conductivities: 1.5 and 2.0; and 1.75 and 2.25 W/m°C. The lower value was taken to be characteristic of the dehydrated shale anywhere the temperature exceeded 125°C. Below this temperature, the higher value was used and similarly did not change with temperature. The intervening hole between the packer[1] and the heater top was assumed to have a wall temperature of 100°C, and in the vicinity of the heater, actual heater surface temperatures were used. Both isotherms and input wattages were computed for the full 8-month duration of the test. Thermal decay of both sites was then modeled for the 2 months following power cutoff.

From the above study, it became apparent that isotherm positions were far less sensitive indicators of in situ thermal conductivity than were heater wattages. For example, it was difficult to determine whether the actual isotherms measured in the field more closely matched those modeled using 2.5 or 2.0 W/m°C (Figure 14). However, when heater wattage was plotted against assumed thermal conductivity, there was a substantial spread between the output expected for different modeled conditions (Figure 15). Also shown in Figure 15 are the Site 1 heater wattage and the required wattages calculated for the two split conductivities that were modeled. It is apparent, based on heater wattage, that, late in the test, the Site 1 power was characteristic of an average conductivity of about 1.8 W/m°C, while early in the test, a value as high as 2.3 W/m°C was appropriate. The two split conductivities had power outputs that plotted close to the average conductivity of each pair. Thus, while a great drop in conductivity within the 100°C isotherm can be ruled out on the basis of the temperature gradient immediately adjacent to the heater [Figure 3(a)], a modest increase or decrease of conductivity in this region would still give "reasonable" average conductivities for the formation and therefore would not be detectable with the thermocouple array used in this test. An additional point deserving discussion is the spatial disagreement between the computed and actual 40° and 50°C isotherms that

appears in the upper part of Figure 16. The computed temperature profile indicates more rapid heat transport than the profile measured in the field. The explanation for this is probably that the modeled hole-wall temperatures above the heater (100°C) were too high. Had lower hole-wall temperatures been used in the model, the predicted heater wattages would have fallen; hence the figure of 1.8 W/m°C cited earlier was a slightly conservative value for in situ conductivity.

Finally, there is the role played by boiling water. At the conclusion of the test, there was an upward displacement of actual isotherms for temperatures at or above 100°C when compared with isotherms computed on the assumption that conduction was the only mode of heat transfer. The effect, however, is not as pronounced as was reported for earlier times. That is, the boiling of water in and beneath the hole bottom arrested the downward migration of isotherms below the heater, while rising steam carried additional energy to the region above the heater. (See lower part of Figure 16). In all probability, this reflects both the permeability decrease caused by the heating cycle and the fact that, during the last months of the test, the bottom of the Site 1 heater was above water. Consequently, it is unlikely that, during this period, boiling groundwater in direct contact with the heater skin was supplying steam to the upper part of the hole.

An idea of the total amount of energy that was consumed by the boiling of groundwater may be gained from the amount of scale deposited on the bottom of the Site 1 heater. Assuming the hole bottom was filled to a depth of 2.0 cm with a layer that was 50% (by volume) anhydrite, it follows that roughly 33 moles of anhydrite were deposited from solution. Since the calcium concentration in post-test groundwater was found to be roughly 10^{-2} moles per litre, it follows that the vaporization of about 1,900 litres of water would be required to deposit the anhydrite. To vaporize this amount of water requires about 4×10^9 joules or roughly 12% of the total energy fed into the formation during the 243 days of the test. This computation does not include the possibility that steam may have condensed and returned to the hole bottom as distilled water. Such an occurrence is highly unlikely, however, since over the heater length, the hole walls were considerably above the boiling point of water. Thus, refluxing liquid water could only reach the hole bottom by going through the formation, in which case it would be likely to equilibrate with limestone.

Modeling of the cooldown phase of the experiment was not successful. In general, the site cooled at a rate that was more rapid than would be predicted from the range in conductivities deduced during the heating phase of the experiment [Figure 17(a)-(d)]. The effect was most pronounced in the region immediately above the heater (Figure 18), probably because of the discontinuation of steam generation beneath the heater. On the heater midplane, there was also a tendency for the 0.61-metre thermocouple to cool more rapidly with respect to the modeled curves than the more distant thermocouples. Finally, as noted previously, no rapid quenching occurred when the temperature dropped below the boiling

point of water. It follows that quenching of the site by groundwater did not play a major part in heat dissipation during site cooldown. This conclusion is in agreement both with the very low permeabilities noted for the formation at the conclusion of the test and with the observation that at Site 2 the air pressure had been removed from the heater hole for several weeks before water was seen to collect in the bottom of the hole.

Mechanical Response Modeling

Mechanical response modeling in the Conasauga Experiment was directed toward two objectives: first, field test data required interpretation; second, it was desirable to ascertain what differences might be expected if the experiment had been done at depths appropriate for an actual repository.

Interpretation of field test data largely been covered in the preliminary results report.[1] Briefly, it was our that the vertical extensometer data were characteristic of a positive thermal expansion. This result was somewhat unexpected because, in the laboratory, shale samples have usually shown marked thermal contraction due to dehydration of the clay minerals at around 100°C.[1] The discrepancy was probably caused by the extensometers having been located in regions where the temperature was characteristically below 120°C, a border region between hydrated and dehydrated shale. A net behavior resembling overall expansion resulted.

The other concern pertaining to the mechanical response of the formation was that of crack generation. No new cracks were visible in the actual hole walls, presumably because of the already fractured nature of the rocks in the region. That is, a few small cracks would never have been noticed among the many already present, and the subdivision of the rock into many small domains precluded transmittal of tension stresses over long enough distances to allow generation of large, easily discernible cracks. In addition, extensometer data indicated that the formation as a whole experienced a modest "expansion," which could have closed small cracks that opened because of local contraction. Such behavior is consistent with the decreased permeability noted in post-test transmissivity measurements.

In analyzing the effects of a heat source placed at depth, as opposed to the near-surface heater experiment environment, the following tactic was taken. In accordance with specifications shown in Reference 5, the depth of the repository was assumed to be roughly 430 metres. A heat source 3 metres long was assumed to be implanted in a hole 7 metres deep centered in a room 3 metres in radius and 7 metres high (Figures 19 and 20). Time-dependent temperature fields from Site 1 were used in all cases. Three cases were considered: the near-surface heater experiment, a repository at depth, and a room having the above geometry but without any in situ stress. The latter analysis was performed so that geometric effects could be sorted out from those resulting from the burial depth. The analysis of the heated region was based on a two-dimensional, axisymmetric,

finite-element simulation using the BMINES finite-element code[6] to provide additional insight into the effects of burial in a long room. Tunnel floor motion was also investigated on the basis of a plane strain analysis. The shale was assumed to be isotropic and elastic and to have the properties listed in Volume 6 of Technical Support for GEIS: Radioactive Waste Isolation in Geologic Formations, titled "Baseline Rock Properties: Shale." (See also Reference 5.) The investigators are aware that the Conasauga shale is neither isotropic nor strictly elastic; but lacking actual material properties and a model capable of handling many thousands of layers of different materials that are folded and fractured in a variety of directions, the simulation provided the best approximation that could be made within the time frame of the experiment.

On the basis of the analysis the following generalizations seem warranted:

1. Beyond a distance of about three heater lengths, the assumed boundary conditions had a negligible effect on the stresses or displacements calculated by the model.
2. A parametric study using realistic variations in material properties showed that a significant range in anticipated deformation fields was plausible.
3. Stress changes and deformations induced by the heater were very localized. For example, radial stress was reduced to a fifth of its maximum value in 5 metres. The hoop stress was reduced to a sixth of its maximum in 2 metres and to zero in 4 metres. Radial strains fell to negligible values in 3 metres.
4. In the comparison between near-surface and tunnel experiments, only slight differences were noted in stress fields induced by the heating process, and the same generalization applies to radial deformations (Figure 19). Significant differences, however, were noted in vertical deformations. The presence of a room allowed much more vertical motion above the heater, but motion below the heater was essentially the same (Figure 20).

The analysis did not include pressure dependence of the elastic properties. Hence, if the pressure dependence of the material is small and the deformation elastic, the stresses and radial deformations induced in the material around a heater emplaced near an underground room should be quite similar to those measured in a near-surface environment.

Analysis of Geologic Materials

As was pointed out in the discussion of post-test coring activities, only minor changes were induced by heating. This result was not wholly unexpected. A large body of geologic literature attests to the occurrence and stability of clay minerals in a wide variety of environments and to the extremely sluggish kinetics of reactions involving the breakdown of silicate lattices. In regions where temperatures were highest and the departure from initial conditions greatest, the pressure was insufficient to maintain a liquid phase. Consequently, in regions

most prone to mineralogic change, the additional constraint was imposed that reactions involving two or more minerals as reactants must proceed via the mechanism of solid-state diffusion. A variety of techniques was nevertheless employed to evaluate the subtle changes that did occur.

1. Differential Thermal Analysis

Typical differential thermal analysis (DTA) data for the primary rock types at the site are illustrated in Figure 21. The basic features of Figure 21 are (A) loss of bound and unbound water between room temperature and 150°C and (B) the oxidation of pyrite and ferrous iron in silicate minerals at about 350°C. Finally, at about 475°C the clay minerals themselves start breaking down slowly to liberate water (C). In siltstone or limestone samples, the proportion of clay is significantly smaller, and these reactions appear less prominently in the DTA traces. Since the maximum temperature experienced adjacent to a heater was generally less than 385°C, it follows that water loss and oxidation are the major changes that would be expected in the field.

2. Grain Density and Specific Surface Area Determinations

Although no major changes can be expected in the phases present in Conasauga samples, the possible combined effects of heat, oxidation, and dehydration on the submicroscopic fabric of the rock are less clear. Although no progressive changes were evident in grain densities (Table 1), it is apparent that the specific surface areas of samples taken adjacent to the heaters (denoted by an asterisk) were generally less than the areas determined on pretest samples or samples taken from localities farther from the heater that had remained relatively cool. It has not been possible, however, to ascertain whether this represents a recrystallization of the finest grained fraction or decreased permeability induced by soluble mineral precipitation and/or sample compaction.

3. Microscopic Examination

The term "Conasauga shale" is, to a degree, a misnomer. In addition to the numerous obvious interstratified layers of limestone and siltstone, the great majority of the "shale" units themselves contain a substantial proportion of silt-size particles. Examination of thin sections has therefore been more fruitful than would be anticipated had the shales consisted almost wholly of particles 2 microns or less in size. Briefly, in thin section, the shale units exhibit a strong sinuous fabric due to the orientation of the (001) crystallographic plane parallel to bedding in both the fine-grained clays and coarser grained chlorite (Figure 22). A similar effect is found in the coarser grained siltstone layers (Figure 23). Within shale-rich layers, it is common to observe ellipsoidal clusters of coarser quartz and chlorite grains surrounded by an anastomosing accumulation of darker, fine-grained clay minerals, which reflects the pervasive small-scale shearing and fracturing that occurs in the formation. On occasion, layers are offset by a fracture or several en-echelon shear planes trending obliquely to the layering of the formation (Figure 24). A clean break may occur (Figure 25), but in shale, the fracture commonly disappears or bifurcates into fractures and shears that are soon lost in the fabric of the shale (Figure 26).

Table 1

Grain Density and Specific Surface Area Determinations of Conasauga Shale Samples

S1-4 Pretest			S7 (0.54 m from site center) (Site 1 post-test)			S10 (0.67 m from site center) (Site 2 post-test)			S1-1 (Site 1 post-test)			S2-1 (Site 2 post-test)		
Depth (m)	ρ (g/cm^3)	A (m^2/g)	Depth (m)	ρ (g/cm^3)	A (m^2/g)	Depth (m)	ρ (g/cm^3)	A (m^2/g)	Depth (m)	ρ (g/cm^3)	A m^2/g	Depth (m)	ρ (g/cm^3)	A (m^2/g)
12.0	2.74	6.0	8.6	2.75		15.2	2.79	-	13.8-15.4	2.84	-	*16.6-17.5	2.93	7.01
12.5	2.85	-	10.5	2.76		*15.5	2.73	2.72	-	-	-	*15.1-16.9	2.82	5.27
13.2	2.93	11.7	10.8	2.83		*16.0	2.84	4.75	-	-	-	*Heater Bottom	2.84	1.75
13.8	2.74	-	11.2	2.71	13.4	*16.8	2.75	-						
14.3	2.72	-	*12.2	2.78	3.2	*17.0	2.89	-						
15.1	2.79		*13.4	2.78		18.5	2.90	14.1						
16.5	2.76		*13.7	2.73	2.5	-	-	-						
18.5	2.75		*14.1	2.75	-	-	-	-						
-	-		*15.0	2.75	-	-	-	-						
-	-		16.5	2.74	-	-	-	-						
			17.5	2.87	8.5	-	-	-						

Legend:

* Denotes sample at the same depth as a heater (and which, therefore, experienced significant heating).

ρ Grain density of dried, powdered samples, determined on a Micrometrics Automatic Pycnometer, Model 1310.

A Specific surface area of chip samples, determined on a Micrometrics Orr Surface Area--Pore Volume Analyzer, Model 2100 D.

At Site 1, the predominant rock types were a dark gray shale, occasionally calcareous and showing relic fossils (Figure 27), and a silty limestone interspersed in beds ranging in thickness from several millimetres to several centimetres (Figure 24). At Site 2, variegated shales and siltstones were more common. Except for fracture fillings, calcite was less common at Site 2 than at Site 1. The general mineralogy at the sites was similar to that described in the literature for the upper part of the middle Conasauga Formation.[7]

Textural Changes -- With this information as background, comparisons may be made between the texture of shale samples exposed to heating (Figures 28 and 29) and those obtained before heating (Figures 22 through 27). Changes in grain size were not observed, even in the very fine-grained material, and no recrystallation textures were visible in regions composed of silt-size particles. The general fabric of the rock remained unchanged (Figure 28). No evidence was found that indicated opening along bedding planes separating strata of different rock types or around knots of more competent material or fossils embedded in shale units. The numerous shear planes in the rock also seemingly had remained closed, as mentioned previously. However, a myriad of hairline fractures that were open before the test served as conduits for heated air and steam and, consequently, underwent surface oxidation (Figure 29). Both the extent of calcite twinning and the uniformity of extinction under crossed polars in quartz grains are sensitive to stresses experienced by the rock. No systematic changes, however, were observable in either of these parameters.

Optical examination of thin sections is difficult because of the dual limitations of restricted magnification and the requirement that the sample be transparent. The scanning electron microscope, however, is capable of examining opaque samples, has great depth of field, and can give substantially higher magnification than is possible with optical systems. Figures 30 and 31 compare typical fracture surfaces parallel and perpendicular to bedding before and after heating. Also shown are two slickensided surfaces, one before heating and one obtained after the test (Figure 32). The approximate maximum temperature experienced by the sample shown in Figure 30(b) was 200°C, that in Figure 31(b) was 225°C, and that in Figure 32 was 175°C. It is apparent once again that the heating cycle did not disrupt the fabric of the rock. In short, neither the effects of recrystallization of fine-grained material nor heat-induced stresses have appreciably altered the rock.

Mineralogical Changes -- The most pronounced change induced by heating of the rock was that of iron oxidation. Although most obvious along hairline fractures (Figure 29), the change was evident wherever the temperature exceeded the boiling point of water. In the bulk of the rock, oxidation imparted a general tannish tinge, a result of partial oxidation of pyrite and ferrous iron in the finest grained clay fraction (Figure 28). Under conditions of marginal oxidation, the coarser grained chlorite may retain its characteristic green color or begin to acquire a yellowish tinge indicative of partial oxidation. In a post-test core taken from a radius of 0.54 metre at Site 1, this discoloration extended from 11.4 to 15.7 metres of depth, while in a core from 0.67 metre at

Site 2, the discoloration extended from 12.3 to 19.4 metres of depth. The somewhat greater vertical extent at Site 2 is undoubtedly a reflection of the greater air pressure and consequently of the greater availability of oxygen adjacent to the heater hole. At still higher temperatures, the chlorite is oxidized to a brick-red color, and the pyrite is more severely affected.

4. X-Ray Diffraction of Bulk Samples

An elaborate series of tests exists for detecting changes in the structures of clay minerals. Based on a series of X-ray diffraction peaks corresponding to the (020), (110), and (111) reflections, a crystallinity index for kaolinite has been defined.[8] The various mixed-layer clays that occur during the progression from illite to montmorillonite, as well as the additional complications arising from introduction of chlorite layers, are treated in the literature.[9,10,11] Particularly useful as diagnostic tools are the (001), (002), and (003) peak positions and the degree to which these diffraction peaks shift when interlayer water is replaced by ethylene glycol. To apply these techniques, however, requires a relatively simple mixture of clays, since reflections from one type of clay often overlap those of another.

The Conasauga shale is, unfortunately, far from a simple mixture of clays. Kaolinite, chlorite, and illite all occur in significant proportions. Further, the illite has a poorly defined structure that gives a diffuse (001) diffraction peak extending from 10 to 11 Å. From the consistent 5.00-Å-peak position and the presence of a consistent 10.00-Å leading edge on the illite peak, it may be inferred that the illite contains less than roughly 15% expandable layers. It is also possible that the illite may contain some water trapped in nonexpandable layers, either in interlayer structural positions not occupied by potassium or as lenses of water. This has been proposed as a possible explanation of why illitic clays fail to respond to glycolation but nevertheless show a broad peak that centers on 10.05 Å,[11] a characteristic exhibited by many, but not all, Conasauga samples. In short, from sample to sample, it was found that the Conasauga consists of a heterogeneous assemblage of clay minerals, the proportions and compositions of which are highly variable.

In light of the inherent differences between samples, it is not surprising that trends induced by heating were difficult to assess. Oriented X-ray diffraction mounts were nevertheless prepared from roughly the same stratigraphic levels on cores taken before and after the test. Comparisons were also made between glycolated and unglycolated samples. It was generally apparent that none of the principal silicate phases was greatly affected by the heating cycle. No consistent sharpening of either the kaolinite or chlorite peaks was noted. The illite peak at 10 Å remained broad, and the (002) peak remained sharply fixed at 5 Å. No consistent change in response to glycolation was visible in either heated or unheated samples. The only change that was even perceptible at the conclusion of the field test was a slight accentuation and sharpening of the mixed-layer clay peaks lying between 10.3 and 11.0 Å. It was found however, that post-test samples

taken from S7 and S10 showed development of gypsum peaks, the strongest of which were located adjacent to and slightly above the level of the heater. Presumably, this gypsum was formed as a consequence of pyrite oxidation.

5. Fracture Surface Mineralogy

In contrast to the tan discoloration exhibited by bulk samples, the wall of the heater hole and hairline fractures along which heated air and steam circulated were colored a bright brick red. In this section, it could be observed (Figures 28 and 29) that, even in very fine-grained, impermeable material, this discoloration extended into the rock roughly 0.1 mm from the fracture surface. Such extreme coloration, however, did not appear to alter the rock texture. At Site 1, this type of coloration was restricted to the hole walls themselves. At Site 2, sufficient air escaped along open cracks that the reddish coloration of these surfaces persisted to roughly the location of the 70°C isotherm.

In studying fracture surface mineralogy, there was the possibility of finding phases formed from soluble and hence mobile constituents, as well as from the insoluable silicate minerals characteristic of the bulk rock. Both pre- and post-test samples were examined using a binocular microscope, and scrapings were examined optically as well as by X-ray diffraction (Table 2). Gypsum was rarely observed by optical means in pretest samples and did not appear at all in X-ray diffraction patterns made of pretest fracture surface coatings. Heating apparently oxidized a significant amount of pyrite, resulting in the wide dispersal of gypsum. The oxidation of pyrite in a steam-laden atmosphere may liberate two sulfuric acid molecules for every FeS_2 group oxidized. Calcite ($CaCO_3$), however, occurs ubiquitously throughout the formation and neutralizes the sulfuric acid by the reaction $CaCO_3 + H_2SO_4 = CaSO_4 + H_2O + CO_2$, leaving calcium sulfate and carbon dioxide as evidence of the process. Since the amount of calcite greatly outweighed the amount of pyrite, there was no significant diminution in the calcite detected. At the conclusion of the experiment, $CaSO_4$ hydrated to form gypsum ($CaSO_4 \cdot 2H_2O$) when the temperature fell below about 45°C (Figure 33). It should be added that the gypsum which precipitated in the cracks was not of a form that would account for the marked permeability decrease noted in post-test transmissivity measurements (Figures 34 and 35).

The presence of calcium carbonate also had bearing on the observation that hydrous iron hydroxides were not observed to precipitate from solution in fractures. The pH of water samples measured in the field varied between 6 and 7. Since the solubility product of amorphous $Fe(OH)_3$ is 10^{-38} (Reference 12), it follows that Fe^{+++} is essentially fixed by this solubility limit and that only Fe^{++} could be mobile in such a solution. However, consideration of the reaction

$$2Fe^{++} + \tfrac{1}{2}O_2 + 5H_2O \rightleftharpoons 2Fe(OH)_3 + 4H^+$$

indicates that at 100°C even 1 ppm of Fe^{++} in solution would require substantially less than 1 ppb dissolved oxygen in the ground water,[13] a value that is

Table 2

Mineralogy of Fracture Surfaces Determined by X-Ray Diffraction

	Conasauga Sample I. D.		Barite	Gypsum	Calcite	Quartz	Kaolinite	Illite		Chlorite
	Hole No.	Depth (m)						4.48 Å	10 Å	14.5 to ~15 Å
1)	S1-4	13.2*			stronger than 8	major	med.	med.	weak	weak
2)	S1-4	13.9*			very strong	minor	trace	very weak	trace	trace
3)	S1-4	15.1*			major	med.	weak-med.	med.	weak	very weak
4)	S1-4	15.4*			major	med.	weak-med	med.	very weak	trace
5)	S1-4	18.8*	only							
6)	S1	12.4*			major	med.	weak-med.	med.	very weak	trace
7)	S7	8.7		minor	major	major	med.	med.-strong	weak	weak
8)	S7	8.7			more dominant	minor	weak	weak	weak	very weak
9)	S7	10.5		minor trace	major	probable trace	med.	med.		
10)	S7	10.5		major	major	more dominant than 11	med.	med.-strong	very weak	very weak
11)	S7	11.2		major		major	weak	strong		
12)	S7	11.7		minor	major	possible trace	weak	weak-med.	very weak	very weak
13)	S7	12.3	only							
14)	S7	13.4		major	major	more dominant than 11	weak-med.	med.		
15)	S7	13.7	major	minor	weaker	trace	weak	weak	very weak	very weak
16)	S10	15.2		major	possible trace	more dominant than 11	weak-med.	weak		
17)	S10	15.6	major				very weak			very weak
18)	S10	16.7		major		more dominant than 11	weak-med.	med.	very weak	weak
19)	S10	16.7		major	major	major	weak			trace
20)	S10	18.6		strong-est of all samples		minor	very weak			

*Denotes samples taken before heating cycle.

unlikely considering that air was supplied to the heater holes. Thus, a combination of a pH buffered by the presence of calcite and a moderately oxidizing condition precluded iron traveling in solution and precipitating as a fracture filling. A final point deserving of note is the information in Table 2 regarding silicate minerals. It is almost impossible to isolate fracture fillings without obtaining a small amount of wall material. As such, this is material that experienced the greatest number of oxidizing conditions present in the experiment, and even this degree of oxidation failed to destroy the primary clay minerals present in the formation.

6. Groundwater Analyses

In contrast to the limited capability for detecting changes offered by thin-section examination or analysis of X-ray diffraction patterns, it was possible to analyze water samples for most elements to the parts-per-million range. Such data can provide insight into extremely subtle changes that may result from heating. Analyses were therefore performed for most of the major rock-forming elements (Table 3). Iron, however, was omitted as it was felt that the rusting steel casings emplaced in the drill holes would cause sufficient contamination to make such analyses meaningless. The same reasoning was extended to most trace elements, since fielding the experiment involved a variety of materials which could potentially contaminate the groundwater. To complement the groundwater analyses, two gas samples were recovered from Site 1, one from above and one from below the packer (Table 4). Water temperatures were not measured at the time of sampling, so the temperatures shown in Table 3 are estimates based on the temperatures at comparable points in the formation where thermocouples had been emplaced. One of the more striking regularities shown is the nearly constant calcium concentration. Considering the reaction

$$CaCO_3 + H_2CO_3 \rightleftharpoons Ca^{++} + 2HCO_3^-$$

and using the average values $pCO_2 = 10^{-3}$ MPa (Table 4) and $[Ca^{++}] = 10^{-2}$ M (Table 3), it follows from considerations of equilibrium and relevant thermodynamic data that pH values of 6.9 and 6.6 would be expected at 25°C and 100°C, respectively.[12,13] This observation is in accordance with field measurements made at the time of sample recovery. By the same token, it follows that HCO_3^- concentrations would have values of $10^{-3.0}$, $10^{-3.1}$, $10^{-3.3}$, and $10^{-3.8}$ molar at 25°, 50°, 60°, and 100°C, respectively. Values in Table 3 are somewhat greater than this, probably reflecting the buildup of carbon dioxide between the time the heater hole atmosphere was sampled (18 January 1978) and the months of July through November, when most of the water samples were collected.

The oxidation of pyrite to form calcium sulfate has already been discussed, but it is pertinent to assess whether this occurred to the extent that groundwater in the formation was in fact saturated with calcium sulfate. The product $[Ca^{++}][SO^{++}]$ (Table 3) is plotted against the saturation curves of gypsum, anhydrite, and hemihydrate in Figure 36.[14] It is apparent that, for most samples, saturation with anhydrite was achieved and that the solute concentration generally was equal to or greater than that expected for gypsum saturation. This

Table 3

Groundwater Composition[a] Before and After Heating Cycle

(Concentration in 10^{-3} moles per litre)

Sample Number	Hole of Origin	Sample Date	Temp. (°C)	Ca^{++}	Mg^{++}	Na^{+}	K^{+}	Sr^{++}	Mn^{++}	HCO_3^-	SiO_2	$SO_4^=$	Cl^-	pH
Site 1														
1	S1-1	10/3/78	28	16	9	11	1	0.001	0.01	5	0.7	26	4	6
2	S1-6	8/2/78	65	6	3	3	1	0.006	N.D.	1	0.5	10	0.4	7
3	S1-6	8/3/78	60	6	3	2	0.8	0.009	N.D.	2	0.4	10	0.4	-
4	S1-14	7/28/78	45	12	9	3	0.7	0.005	N.D.	1	0.4	21	0.7	6
5	S1-14	8/2/78	45	11	8	3	0.7	0.006	0.004	2	0.2	20	0.4	7
6	S1-14	8/3/78	45	11	8	3	0.7	0.005	N.D.	1	0.1	20	0.5	-
7	S1-14	8/8/78	45	11	8	3	0.6	0.003	0.007	1	0.1	20	0.4	-
Site 2														
8	S2-1	11/2/78	16	10	70	9	0.9	0.006	0.03	6	0.4	76	3	-
9	S2-3	7/28/78	60-100	13	25	3	0.9	0.006	0.01	4	0.7	36	2	6
10	S2-3	9/7/78	55	14	11	2	0.3	0.008	N.D.	2	0.2	24	0.7	-
11	S2-13	7/27/78[b]	45	14	6	2	0.4	0.015	N.D.	1	0.4	19	0.2	6
12	S2-13	8/2/78	45	14	6	2	0.4	0.016	N.D.	1	0.3	19	0.2	7
13	S2-13	8/3/78	45	13	5	2	0.4	0.015	N.D.	1	0.3	19	0	-
14	S2-13	8/8/78	45	14	6	2	0.4	0.016	N.D.	1	0.3	19	0.2	-
Pretest Samples--1976														
15	River Water[c]	11/20/76	14	0.9	0.1	0	0.4	N.D.	N.D.	2	0.1	0.3	0.1	6
16	X-7	11/20/76	14	2	3	0.9	0.1	N.D.	N.D.	7	0.4	5	0.3	6
17	Average[d]		14	0.8	0.8	0.4	0.08	-	-	3	0.2	0.2	0.08	-

Legend:

N.D. Not Detected

\- Not Analyzed For

[a] All samples contained less than 0.2 ppm Ba, 0.1 ppm Cs and 1 ppm Al

[b] Heater turn-off was 1 August 1978

[c] Taken from reservoir 100 metres from Site 2

[d] Nuclear Fuel Recovery and Recycling Center, License Application, PSAR, DOCKET-50564-1 Table 3.5-8, 1976. This represents the average composition of 15 wells into the Conasauga formation in Bear Valley on the Oak Ridge Reservation.

is corroborated by the fact that the principal component of the scale on the Site 1 heater was anhydrite. All of the anhydrite at the site will eventually hydrate to gypsum, the stable phase below about 45°C, and the solute content of the site groundwater should stabilize at about 0.2 weight percent $CaSO_4$ in solution.

Table 4

Gas Compositions Above and Below Packer at Site 1, 1/18/78

	% N_2	% O_2	% Ar	CO	% CO_2	% H_2O
Above Packer	79.6	16.7	0.85	120ppm	1.0	1.9
Below Packer	75.4	16.2	0.78	160ppm	1.1	6.5
Dry Air	78.1	20.1	0.93	-	0.03	0

Besides calcium, the behavior of two other alkaline earths was also of interest: barium, because barium sulfate occurs naturally as crystals on fracture surfaces, and strontium, by virtue of its importance to nuclear waste management and the fact that it was found in post-test samples but not in samples taken before the heating cycle. Because of the low solubility of barite[12] and the high sulfate concentration in post-test water samples, it was expected that the barium concentration would lie below the limits of detection (0.2 ppm). In fact, no barium was detectable in any of the samples. Strontium, however, was detectable, and it is therefore relevant to ascertain whether saturation had been achieved. From thermodynamic data,[12] it follows that strontium is undersaturated with respect to precipitation of $SrCO_3$ over the temperature range 15° to 100°C, assuming again that $pCO_2 \approx 10^{-3}$ MPa. In the case of the sulfate, it is apparent that at least some of the samples neared saturation (Figure 37).[15,16] Thus, although in this case the source of the strontium was probably limestone in the formation rather than high-level waste, it is apparent that strontium remained in solution despite the presence of clays that presumably should sorb it strongly and that precipitation of the insoluble sulfate could, in fact, serve as a mechanism to retard its migration.

The concentrations in solution of many of the principal cations important in the formation of silicate minerals (Ca^{++}, Mg^{++}, K^+, and Na^+) have increased over what normally occurs in Conasauga groundwater (Table 3). The question therefore arises whether such changes portend alteration of the sediment. Reactions involving minerals are subject to the same equilibrium constraints as other chemical reactions. Thus for example, the change of kaolinite to potassium feldspar may be written

$$Al_2Si_2O_5(OH)_4 + 2K^+ + 4H_4SiO_4 \rightleftharpoons 2KAlSi_3O_8 + 2H^+ + 9H_2O$$

The value for the equilibrium constant is, as always, determined by the relative free energies of the reactants and products; hence;

$$\frac{[H^+]^2}{[K^+]^2[H_4SiO_4]^4} = \text{constant}$$

If the equilibrium is not initially satisfied in the field, the reaction will proceed, at an admittedly unknown rate, until either (1) equilibrium is attained or (2) one of the reactants is totally consumed, thereby eliminating the need to establish equilibrium. The second aspect to be considered is that the value of one or more of the reactants may be fixed by conditions in the field. In the Conasauga test, the pH was constrained by the stipulation that 10^{-3} MPa of CO_2 be in equilibrium with $CaCO_3$, and the silica concentration in solution in most cases was seemingly fixed by equilibration with quartz. Once the number of independent variables has been reduced to two, such as (H^+/K^+) and H_4SiO_4 in the above example, it is then possible to graphically represent the position of the equilibrium boundary.

The mineralogical phases expected to be in equilibrium with an aqueous environment are illustrated in Figures 38 through 45,[17] together with the compositions of water samples taken in the field as represented by their numbers from Table 3. Consider first a single mobile cation, Na^+, K^+, Ca^{++}, or Mg^{++}, in an environment with a pH between 6 and 7 and a silica concentration equal to that found in the groundwater. For sodium and potassium, kaolinite is the stable phase (Figures 38 and 39). For calcium, leonhardite, a calcium zeolite, is predicted to be stable (Figure 40). Most of the points for the Mg system (Figure 41) cluster around the equilibrium boundary between kaolinite and magnesium montmorillonite. However, depending on the temperature at which the water and rock are presumed to have equilibrated, there is also the possibility that magnesium chlorite may become stable.

Multiple cation systems may be investigated by assuming silica activity to be fixed by equilibration with quartz (Figure 42).[18] As would be expected, for the sodium-potassium system (Figure 43), kaolinite is stable. Both illite and kaolinite appear in the potassium-magnesium diagram (Figure 44); however, the illite field never overlaps with the actual water compositions, and kaolinite may or may not be considered stable, depending on which temperature is chosen. From the calcium-magnesium system (Figure 45), it follows that, in fact, the magnesium montmorillonite might be expected to react further to form the calcium zeolite, leonhardite.

In general, predictions based on these diagrams were not borne out inasmuch as the expected reaction products (magnesium montmorillonite and a calcium zeolite) were not clearly discernible at the conclusion of the test. The one possible exception to this generalization was the accentuated X-ray diffraction maxima lying between 10.3 and 11 Å, which may mark the onset of magnesium montmorillonite development. The disagreement between calculated mineral stability and field data arises partly from inaccuracies in the thermodynamic data used and partly from the fact that clay minerals have more complex compositions and structures than were considered in constructing the diagrams. The absence of iron was notable in this respect, as its inclusion in the crystal lattice may considerably broaden the range over which chlorite is stable. However, a portion of the problem certainly could also be ascribed to the

extremely slow kinetics of reactions involving silicates at these temperatures. For example (at least in terms of the diagrams), the mineral assemblages that naturally occur in the Conasauga are also far from equilibrium, and they have had more than 400 million years to equilibrate.

In spite of these limitations, trends in water composition served to underscore the kinds of changes that might be expected with a longer test. Generally, at one extremity of the cluster of points are waters having pretest compositions (Samples 16 and 17), while at the other extremity are the water compositions in one or both of the heater holes (Samples 1 and 8). The points lying between these two extremes represent samples taken from peripheral holes just before or during cooldown. In terms of sodium and potassium, trends are toward sodium montmorillonite or muscovite, respectively (Figure 43). Had conditions existed such that the pH remained constant and either higher silica or alkali metal ion concentrations been generated, there would have been a possibility that the kaolinite already present in the formation might have reacted to form minerals such as these. In the case of the magnesium-potassium system, the trend is toward stability of Mg chlorite (Figure 44). As the temperature increases to 100°C, however, the stability field of magnesium montmorillonite also increases in size. It follows that, between 60° and 100°C, there is a temperature where most of the points would, in fact, lie in the field of a magnesium smectite. In this respect, the general role played by magnesium deserves special consideration. Unlike the other cations considered, relatively small temperature changes greatly alter the conditions under which the various magnesium minerals might be expected to form. In the case of calcium, the trend is from conditions compatible with kaolinite at the ambient ground temperature of 14°C to a situation where kaolinite should be consumed to form a calcium zeolite. Thus, depending on local conditions, the possibility exists for several mineralogic zones to develop over various intervals on a temperature gradient away from a waste canister or other heat source.

7. Waste Form Stability Study

In a dry environment, borosilicate glasses may be expected to devitrify rapidly only at temperatures considerably higher than those of the Conasauga experiment. A considerable body of literature, however, testifies to the fact that both artificial and natural glasses may alter more rapidly in the presence of moisture.[19] A sample of PNL 75-25 waste glass simulant was therefore sandwiched between two pieces of Conasauga core and suspended below the packer in a drill hole 1.3 metres from the central heater hole at Site 1. During the test, the sample presumably was alternately dried and wetted, depending on the availability of steam lower in the hole, and it is unlikely that the temperature was ever much in excess of 100°C.

During the 243-day test, the glass altered perceptibly, forming thin yellowish layers of gel with an aggregate thickness of up to 20 microns (Figure 46). Although the gel was depleted in uranium relative to the glass, elements such as Zn, Ba, and Gd were found throughout the gel, confirming that the coating was

formed by glass alteration rather than by precipitation from the condensation that periodically bathed the sample. No interaction with the rock was apparent; however, the exterior of the gel was covered with a mat of acicular crystals (Figure 47). X-ray diffraction patterns of the altered material showed lines, in general order of decreasing intensity, at $4.28_{(10)}$, $3.07_{(10)}$, $7.60_{(7)}$, $2.10_{(3)}$, $2.88_{(3)}$, $2.32_{(2)}$, $2.69_{(2)}$, $2.21_{(1)}$, $1.9_{(0.5)}$, $1.81_{(0.3)}$, $1.765_{(0.3)}$, $1.539_{(0.3)}$, $3.85_{(0.3)}$, $3.45_{(0.3)}$ Å, where the subscripts represent visual estimates of relative line intensities. Although no phases could be positively identified, gypsum and acmite may account for many of the observed lines.

Beneath the gel, the glass appeared to be fresh. The surface, however, had a scalloped appearance (Figure 48) that apparently mirrored the texture of the overlying gel (Figure 49). Whether spalling of the overlying gel was a consequence of the alternate wetting and drying of the sample or arose due to swelling during initial glass hydration is unknown. It is, however, apparent from the texture of the underlying glass surface that not all the cracking and spalling was an artifact of the dehydration that occurred during preparation of the sample for examination by the scanning electron microscope.

8. Metallurgical Observations

Metallurgical observations made after the Conasauga test may be divided into two categories: those related to test coupons affixed to the bottom of the Site 2 heater and those made on the test hardware, specifically the thermocouples and heater shell. In regard to the latter type of observation, it is important to remember that at Site 2 standing water was completely excluded from the heater hole, while at Site 1 the bottom few centimetres of the heater were immersed during much of the test. In the chamber above the Site 1 heater, therefore, considerable steam condensed and ran down the test hardware.

Dealing first with the metallurgical coupons, a number of candidate canister alloys were evaluated by welding a SS-304L plate, on which alloy coupons had been mounted, to the bottom of the Site 2 heater. The coupons were machined from 0.64-cm-thick plate to be 3.8 cm in diameter and were fastened with SS-304 screws to the plate. Alumina washers were used behind the coupons and under the screws to electrically isolate each alloy.

Unfortunately, the Site 2 heater hole was dry, so the specimen was exposed only to hot air containing very little water vapor. Post-mortem observations made on the coupons are summarized in Table 5. Only the alloys with poor high-temperature oxidation resistance showed any attack, and even this was minimal.

Table 5

Status of Candidate Canister Coupons Exposed to Hot, Dry Conasauga Formation*

Alloy	Oxide Penetration (mm)	Remarks
1018 Steel	0.05	Significant oxidation
4130 Steel	0.02	Significant oxidation
Kovar	0.02	Significant oxidation
Aluminum 2024	0.003	Significant oxidation
SS-20C63	nil	Gold tarnish
SS-Nitronic 50	nil	Gold tarnish
Titanium	nil	Blue tarnish
Zirconium	nil	Tarnish
Inconel 600	nil	No oxidation product
Hastelloy C-276	nil	No oxidation product
MP 35N	nil	No oxidation product

*Reported by J. W. Braithwaite and W. L. Larson, private communication, February 1979.

The test hardware at Site 2 behaved in the same manner as the metallurgical coupons. Corrosion resulted in a uniform oxide coating on the external surface of the heater, grading from a rich copper red at the hottest parts of the heater to a silver metallic surface on unheated parts. The differing conditions at Site 1 resulted in substantially more varied behavior. Beneath the thicker portions of the scale (Figure 8), the heater generally had a silvery appearance except for dark green to rust-colored water marks formed where the scale had pulled away from the heater. The scale itself was generally a light cream to white color except where the inner surface was similarly discolored by water marks. Where the scale thinned, the heater was usually protected until the scale thickness was less than about 1 mm, at which point localized spot corrosion became prominent (Figure 8). The medial portion of the Site 1 heater was corroded in a relatively uniform manner. The upper 0.3 m of the heated section and the upper 0.6 m of the heater body (the terminal section), however, showed more intense corrosion. A stainless-steel shim-stock collar ringing the top of the canister was pitted through in places, and thermocouple sheaths above the heater had been corroded completely for a distance of roughly 1 metre (Figure 50).

The intense corrosion on the upper part of the thermocouples was investigated in some detail, and it was found that stress corrosion cracking was at fault. SS-304L can be susceptible to localized attack by pitting, crevice corrosion, and, worst of all, by stress corrosion cracking in many aqueous environments. Stress corrosion cracking is a synergistic combination of stress and corrosion which produces transgranular cracking at very low stress levels.

Cracks can extend at velocities up to 0.2 mm/h. In order for SS-304 to stress-corrosion crack, the following factors must all be present: (1) tensile stress (residual or applied), (2) aqueous phase, (3) chloride or hydroxide anions, (4) temperature over 60° to 100°C, and (5) dissolved oxygen. All were present in the thermocouple sections at the top of the Site 1 heater. The necessary stresses could have resulted either from fabrication of the thin sheaths or from bending of the tubes around the heater shell. The 304 stainless-steel heater shell probably did not fail only because of insufficient tensile stress in the heater wall.

Several thermocouple strings in the formation also failed during the test. These were emplaced by first fastening them to a piece of PVC tubing and then grouting the entire assemblage into the drill hole. In doing so, however, conditions were generated that accentuated corrosion of the 304 stainless-steel sheath. The PVC may be presumed to liberate some chloride upon heating; however, the greatest effect probably resulted from the basic environment created by the grout itself. A sample of grout placed in contact with deionized water developed a pH in excess of 11 and retained this pH despite being boiled in solution for 2 months in a stainless-steel pressure cooker. A basic environment was also observed to accompany grout in the field. Circulation water used in drilling out the grouted casings developed a pH more basic than 11. Thus, although none of the failed thermocouples could be recovered from the formation, it is plausible to presume that they failed due to a combination of stress and caustic corrosion cracking enhanced by both the presence of a high chloride concentration and a basic environment.

IV. SUMMARY AND CONCLUSIONS

Despite the fact that this experiment was conducted in a near-surface environment, a variety of observations were made that have direct bearing on the disposal of high-level nuclear waste at depth. Chemical processes will operate similarly in either environment, and the presence of substantial overburden stresses does not a priori preclude the development of formation characteristics at depth similar to those in the near-surface environment. If a repository is sited below the water table, groundwater will always be present to some degree. It is also highly likely that, in a volume of rock large enough to encompass a repository, some regions will either already have, or will develop, fracture systems. The following discussion will therefore elaborate on aspects of the Conasauga test data that may directly affect the conceptual design of either a repository or a prerepository vault test.

In view of (1) the complex nature of most shale units, (2) the limited ability of mechanical models to predict fracture initiation or orientation, and (3) the virtual impossibility of locating joint-size fractures by nondestructive geophysical means, the possibility cannot be disregarded that small-scale fracturing may exist adjacent to high-level waste canisters. An estimate of the perturbation such a change would introduce may be obtained by considering that the thermal data reported here reflect the heat dissipation characteristics of a somewhat fractured, water-saturated material. The effects of convection on heat dissipation were found to be small and localized. Above the boiling point of water, isotherms exhibited a small upward displacement; however, below the boiling point, there was good agreement between actual isotherms and those modeled on the assumption that conduction was the only mode of heat transfer. Geochemical interpretation has indicated that only about 12% of the total energy put into the formation went into the boiling of water in the Site 1 heater hole. It follows, therefore, that even in the presence of a groundwater-filled fracture system, conduction rather than convection was the primary mode of heat transfer. Depending on the method of data reduction, in situ thermal conductivities were found to be between 1.5 and 2.3 W/m°C, and no definite drop in conductivity was found at temperatures above 100°C. For comparison, the highest values determined for small prisms of presumably unfractured shale have been about 2.5 W/m°C. In short, unless a formation became fractured to a greater extent than the Conasauga, such an event would not constitute a serious threat to the heat dissipation characteristics of a repository.

The effect of groundwater may, however, extend beyond its influence on the heat transfer properties of the formation. It may be required that the integrity of a canister be assured for a number of years, and corrosion rates may be markedly influenced by the presence of groundwater. The differences noted between the two Conasauga heater sites graphically illustrate the importance of

taking this variable into account. Site 2 may be characterized as "dry," while, at Site 1, the bottom of the heater was immersed in groundwater for much of the test. At Site 2, a uniform reddish brown discoloration of the 304 stainless-steel heater was the only corrosion visible on the heater. A suite of metal coupons affixed to the heater base also showed negligible corrosion. At Site 1, corrosion was more pronounced. Small blotches of intensified corrosion were noted on the top of the heater where abundant steam apparently condensed and collected. More spectacular, however, was the stress-corrosion cracking of a string of thermocouples sheathed in 304 stainless steel. Thus, it was not the highest temperature regions which experienced the greatest corrosion, but the regions where steam condensed and liquid water collected on metal fittings.

A second metallurgical observation concerns the failure of a number of thermocouples in the formation. They were grouted in place, which precluded heat transfer by refluxing of steam. This act, however, created a condition that is highly corrosive to stainless steels. Grouts, and cements in general, induce a strongly basic environment when they set. This factor, in conjunction with injection of oxygen-rich air into the formation, resulted in rapid corrosion rates. It should also be added that a basic environment of this nature will be highly corrosive to glasses in general, and specifically, to borosilicate glass waste forms. It follows that, before cement is used either in a repository or in a vault test, the consequences of creating a localized basic environment should be assessed.

A third lesson may also be learned from the Site 1 heater. The lower part of the heater was protected by scale deposited from the boiling groundwater. Beneath the thicker portions of the scale, the heater was generally unrusted, and the only evidence of corrosion was an occasional gray-green discoloration on the inner surface of the scale. In spite of its beneficial effect on corrosion rates, such scale could create a difficulty in an actual repository. Up to 2.5 cm of scale was deposited on a 3-inch collar beneath the heater. By virtue of its porous nature, such an accumulation on the side of a canister could act as an insulator, causing waste temperatures to reach values higher than anticipated on the basis of formation thermal conductivities. In addition, in trying to recover the Site 1 heater, it was initially found that the boot of scale had securely cemented the heater to the hole bottom. Fortunately, the heater was loosened by reinvading groundwater. In an actual repository, the formation of such a scale deposit could increase the difficulty of recovering a waste canister.

If all other confinement systems fail, the integrity of a repository may depend on the stability of the waste form itself. In a water-free environment, borosilicate glass waste forms may be expected to undergo rapid changes only at temperatures much greater than those presently being planned for high-level waste (HLW) repositories. Water, however, may greatly alter the rate at which glasses are degraded, as indicated by the samples of PNL 75-25 borosilicate glass waste-form simulant that were included in this test. As a consequence of the treatment received during the test, thin, yellowish layers of gel formed on the glass in an aggregate thickness of about 20 microns. Beneath the gel, the glass appeared to

be fresh, but the surface was scalloped in a manner reflecting cracks that had formed during various stages of alteration. It would appear, therefore, that the protective properties of a surface gel may be weakened by alternate drying and wetting such as occurred during this experiment.

In conclusion, in terms of thermal and mechanical responses, data gained during this experiment reflect favorably on shale as a waste disposal medium. The experiment also illustrates, however, that, in virtually all geological settings, there are a variety of nonequilibrium, localized processes that could compromise a sequence of engineered barriers, if not the final far-field geological barrier. The periodic availability of groundwater may cause temperature cycling, allowing for alternate wetting and drying of both the waste and canister. Thus, protective coatings that normally would prevent protracted alteration or corrosion may crack or spall to the extent that rapid degradation of these materials results. In a relatively short time, therefore, the waste form or the canister might cease to act as an effective barrier to the dispersal of radionuclides. Groundwater in immediate proximity to a waste canister will not necessarily be buffered by the same mineralogic constraints that determine the composition of the overall formation waters. Relatively rapid redox and exchange reactions can considerably increase the ionic strength beyond that of normal groundwater. This effect may be compounded by interactions with common construction materials used in a repository or experimental design. These changes also may result in enhanced canister corrosion and waste-form alteration and perhaps may even assist in complexing solubilized radionuclides. The presence of a temperature gradient implies another nonequilibrium condition that must be reckoned with. Although attainment of silicate equilibria is slow, the possibility exists that at least several different assemblages of minerals may develop at different temperatures around a waste canister.

Covering a much shorter time span are concerns related to the movement of groundwater in a temperature field. Boiling around a partially submerged canister may deposit scale, particularly under conditions where heat has resulted in increased solute concentrations. At the other end of the temperature field, condensation may very nearly approximate deionized water, a substance that has been found effective in leaching borosilicate glass waste simulants. Further, if condensation is accompanied by a small amount of oxidation, cation hydrolysis may impart a distinctly acidic condition to the condensate. Finally, the presence of an electrical conductor, such as a metal canister, in a temperature field may generate a condition where part of the element can behave as an anode and part as a cathode. This effect may be particularly pronounced if a portion of the canister is at times submerged and may greatly shorten canister life.

In short, gaining an idea of the general thermal and mechanical response of a rock unit is but the beginning. It is necessary to look beyond the possibility of repository failure arising from an acute thermal runaway or massive fracturing and to consider the potential effects of a variety of subtle, localized, nonequilibrium processes.

References

[1]J. L. Krumhansl, Preliminary Results Report: Conasauga Near-Surface Heater Experiment, 1977, SAND79-0745 (Albuquerque: Sandia Laboratories, June 1979).

[2]A. C. Arthur and C. O. Duimstra, private communication, October 1978.

[3]R. D. Klett, Krypton-85 Disposal Program Semiannual Report, August 16, 1977--March 31, 1978, SAND78-1667 (Albuquerque: Sandia Laboratories, February 1979), App. K, pp 69-77.

[4]Chrysler Improved Numerical Differential Analyzer, TN-AP-67-287 (Chrysler Corp. Space Division, October 1967).

[5]"Drawings for Repository Preconceptual Design Studies: Shale," vol 13, Technical Support for GEIS: Radioactive Waste Isolation in Geologic Formations (Oak Ridge, TN: Union Carbide Office of Waste Isolation, April 1978).

[6]J. R. Tillerson and M. M. Madsen, Thermoelastic Capabilities for the Sandia BMINES Program, SAND77-0378 (Albuquerque: Sandia Laboratories, 1978).

[7]W. de Laguna et al., Engineering Development of Hydraulic Fracturing as a Method for Permanent Disposal of Radioactive Wastes, ORNL-4259 (Oak Ridge, TN: Oak Ridge National Laboratory, August 1968).

[8]D. N. Hinckly, Variability in "Crystallinity" among the Kaolin Deposits of the Coastal Plan of Georgia and South Carolina in Clays and Clay Minerals, ed E. Ingerson (New York: Pergamon Press, 1963), pp 229-35.

[9]C. E. Weaver, "The Distribution and Identification of Mixed Layer Clays in Sedimentary Rocks," Am Min, 41:202-21, 1956.

[10]J. Hower and T. C. Mowatt, "The Mineralogy of Illites and Mixed Layer Illite-Montmorillonites," Am Min, 51:825-54, 1966.

[11]R. C. Reynolds and J. Hower, "The Nature of Interlayering in Mixed Layer Illite-Montmorillonites, Clays, and Clay Mineralogy," Am Min 18:25-36, 1970.

[12]K. B. Krausopf, Introduction to Geochemistry (New York: McGraw-Hill, 1967), Ap. VII.

[13]H. C. Hegelson, "Thermodynamics of Hydrothermal Systems and Elevated Temperatues and Pressures," Am Jour Sci, 267:729-801, 1969.

[14]E. Posnjak, "The System $CaSO_4$--H_2O," Am Jour Sci 5(35A):247-72, 1938.

[15]G. Strübel, Quantitative Untersuchungen über die Hydrothermal Löslichkeit des Flusspats, Baryts, Cölestins und Anglesits und deren Löslichkeit im Wasser und Wässrigen NaCl--Lösungen zwischen 20° and 10°C," (Dissertation, University of Geissen, Germany, 1962).

[16]P. J. Lucchesi and E. D. Whitney, "Solubility of Strontium Sulphate in Water and Aqueous Solutions of Hydrogen Chloride, Sodium Chloride, Sulphuric Acid and Sodium Sulphate by the Radiotracer Method," J Appl Chem, 12:277-79, 1962.

[17]H. C. Helgeson, T. H. Brown, and R. H. Leeper, Handbook of Theoretical Activity Diagrams Depicting Chemical Equilibrium in Geologic Systems Including an Aqueous Phase at One atm. and 0° to 300°C (San Francisco: Freeman Cooper Co., 1969).

[18]J. D. Holland, "Gangue Minerals in Hydrothermal Deposits," Chapter 9, Geochemistry of Hydrothermal Ore Deposits (Chicago: Holt, Rinehart and Winston, 1967). A compilation of experimental work by Alexander, Heston, and Iler, 1954; Okamoto, Okuna, and Gato, 1957; Van Lier et al., 1960; Morey, Fournier, and Rowe, 1962; Krauskopf, 1956; and Fournier and Rowe, 1962.

[19]R. C. Ewing, Natural Glasses Analysis for Radioactive Waste Forms, Scientific Basis for Nuclear Waste Management (New York: Plenum Press, 1979), pp 67-68.

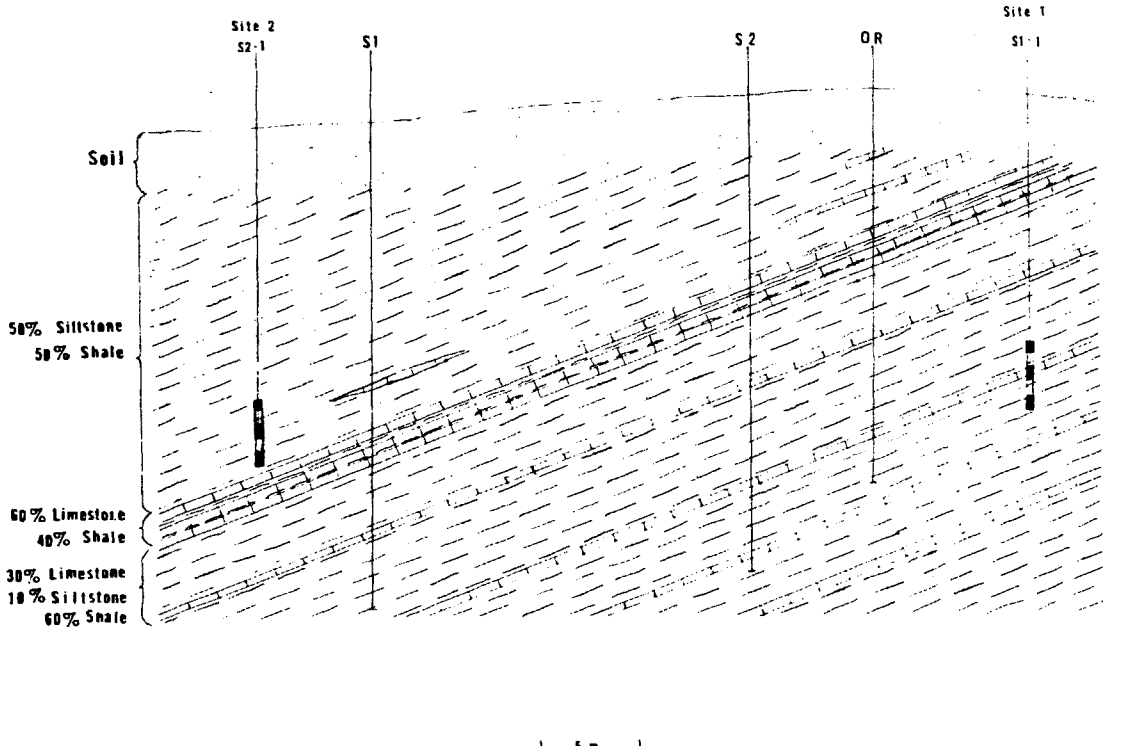

Figure 1. Geologic Section Showing Heater Positions (S2-1 and S1-1) in the Conasauga Experiment.

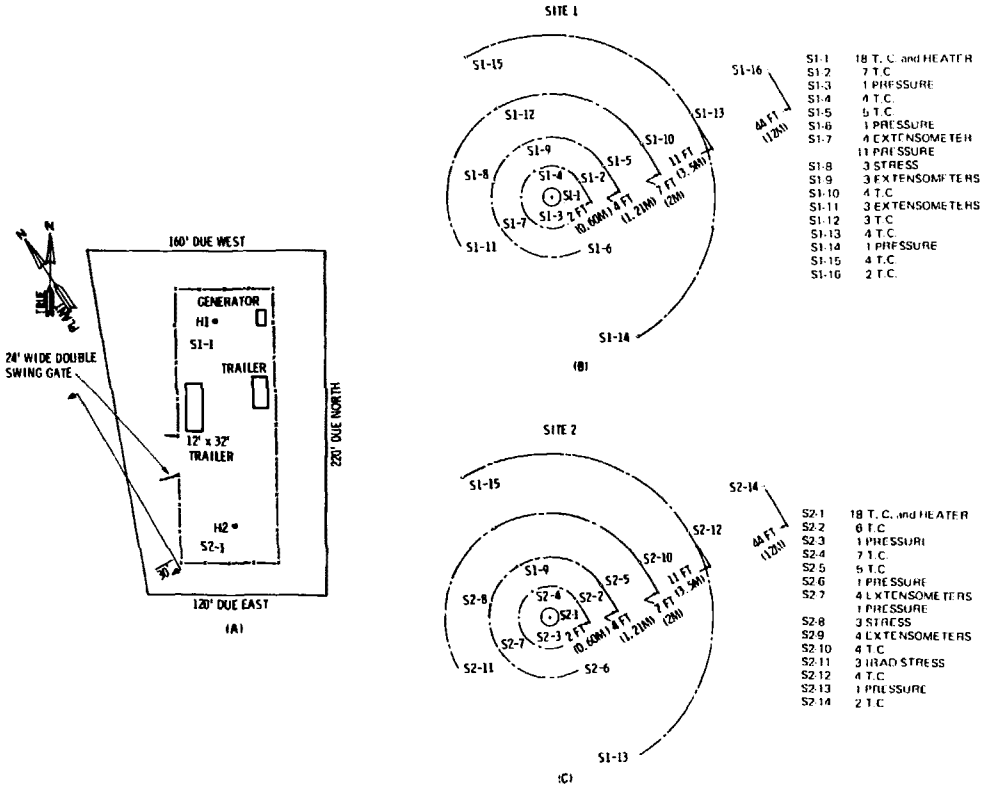

Figure 2. Schematic Diagram of Site Layout for Conasauga Experiment Showing Locations of Heaters, Thermocouples (T.C.), Pressure Gauges, Vertical Extensometers, and Horizontal Stress Gauges

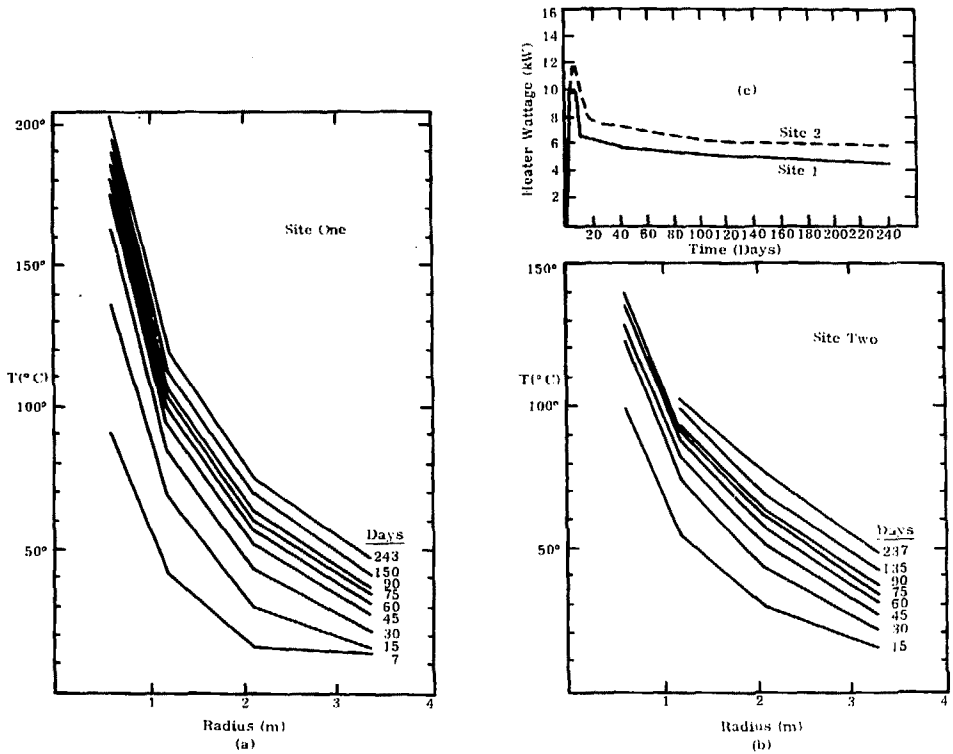

Figure 3. Site Operation Characteristics of the Conasauga Near-Surface Heater Tests

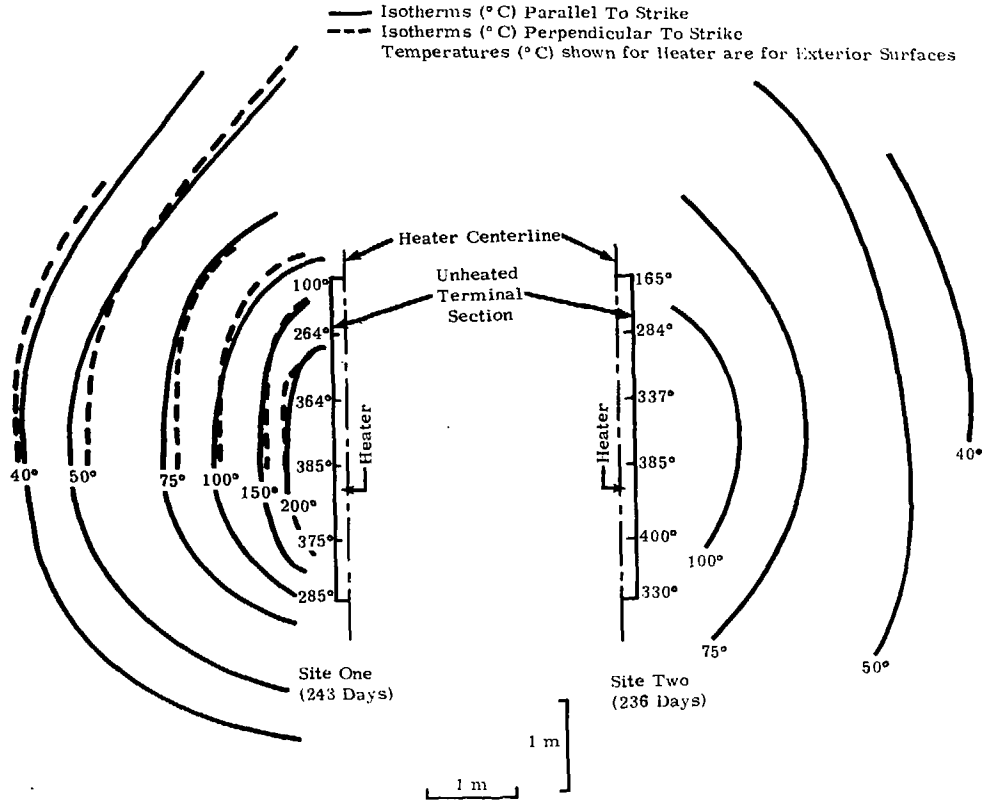

Figure 4. Isotherms at Sites 1 and 2 Just Before Heater Turnoff (1 August 1978)

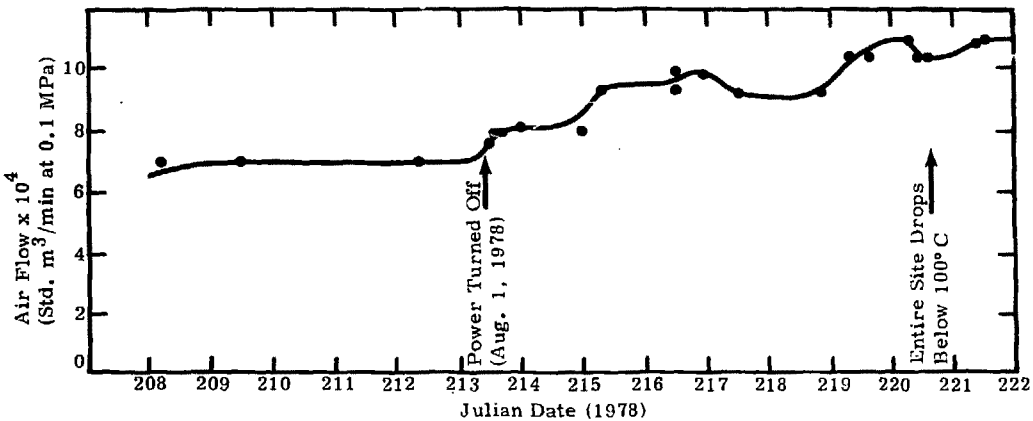

Figure 5. Airflow Required to Maintain 0.08 MPa on the Site 1 Heater Hole

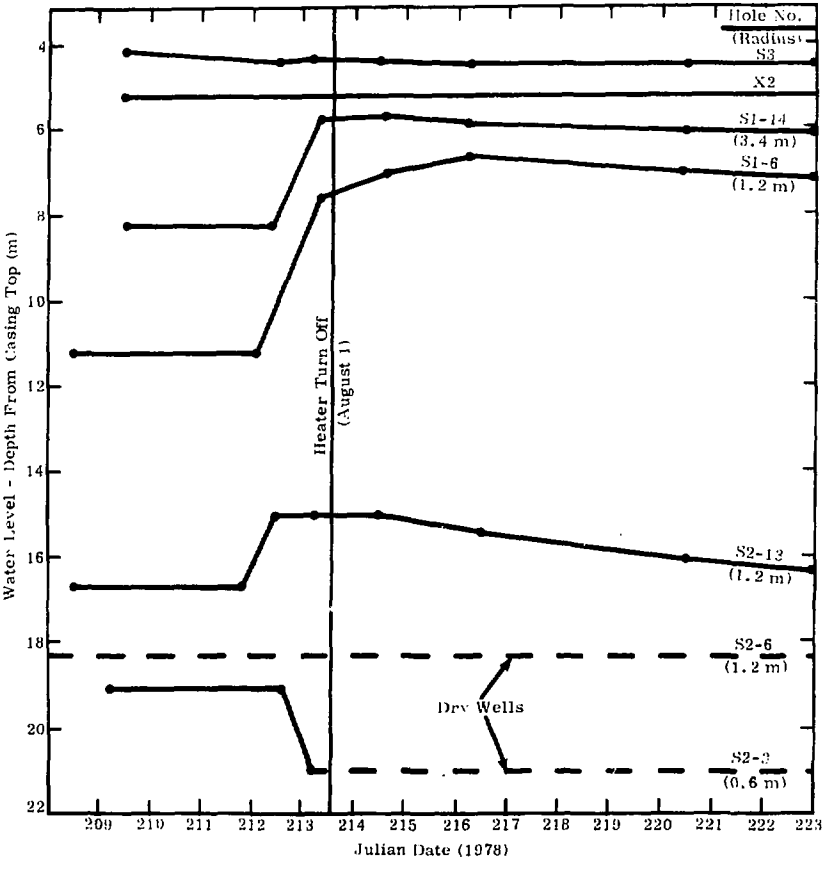

Figure 6. Water in Satellite Holes Before and During Cooldown

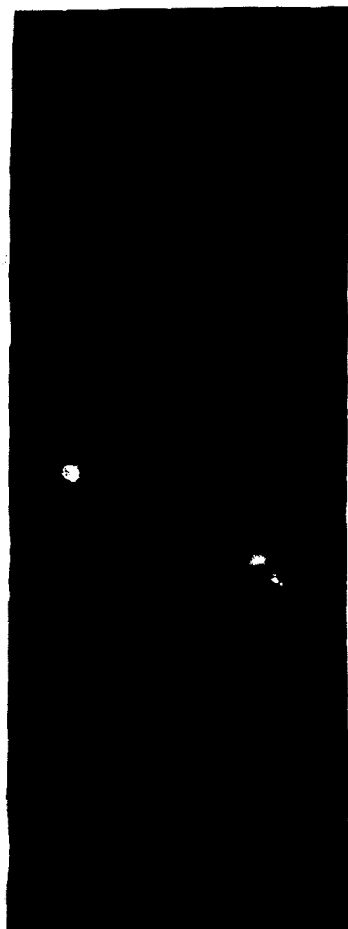

Figure 7. Site 2 Heater After Recovery at End of Test

Figure 8. Lower Part of the Site 1 Heater at Conclusion of Test

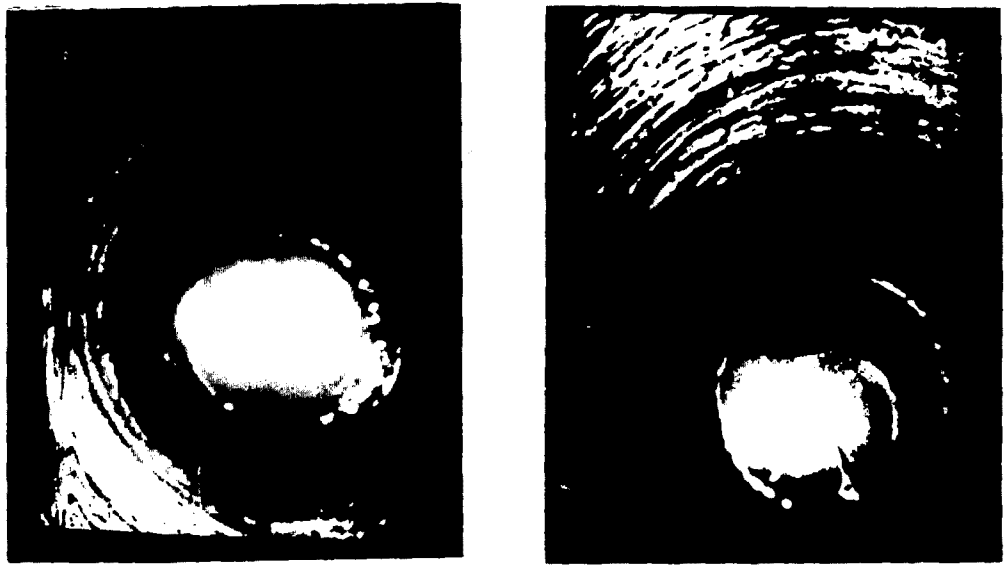

A. Before

B. After

Figure 9. Comparisons at the Site 1 Heater Hole; Camera at 13-metre Depth

A. Before B. After

Figure 10. Comparisons at the Site 2 Heater Hole; Camera at 15-metre Depth

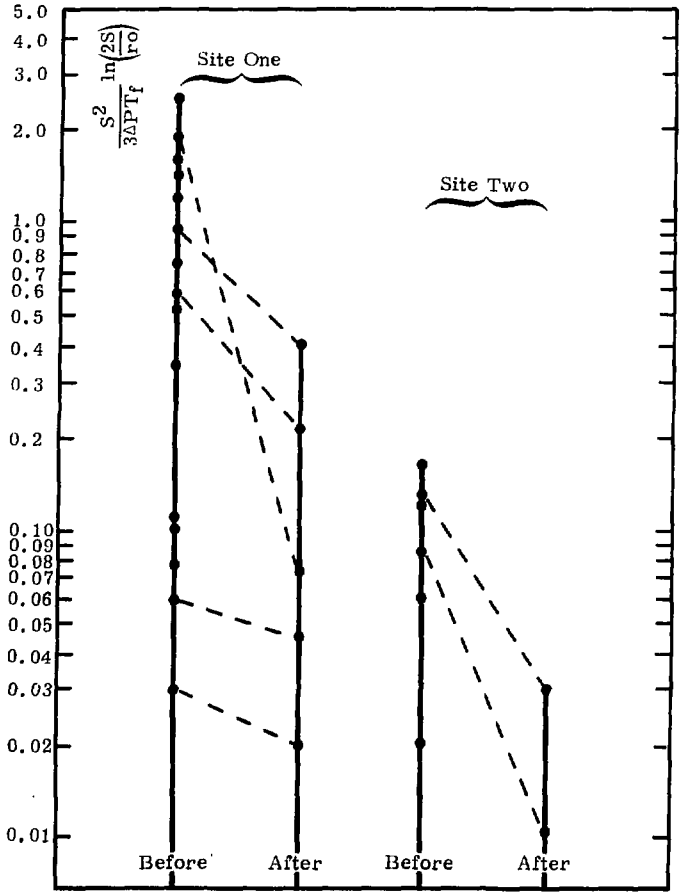

Figure 11. Values of $S^2 \ln(2S/r_o)/3\Delta P\ T_f$ Computed for Various Pairs of Injection and Exit Holes. Dashed lines are equivalent tests.

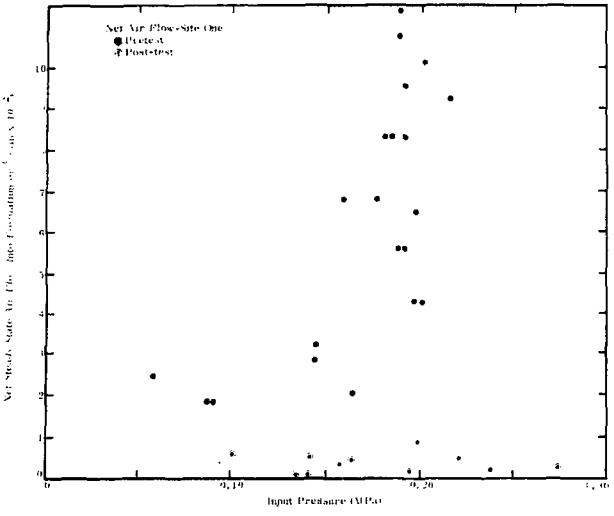

Figure 12. Net Airflow at Specified Pressures for Site 1 Holes

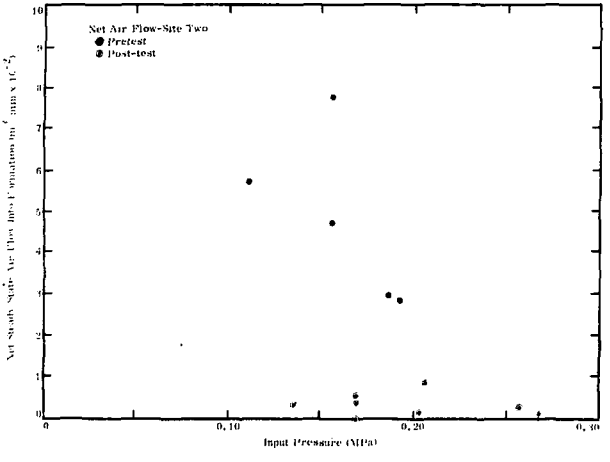

Figure 13. Net Airflow at Specified Pressures for Site 2 Holes

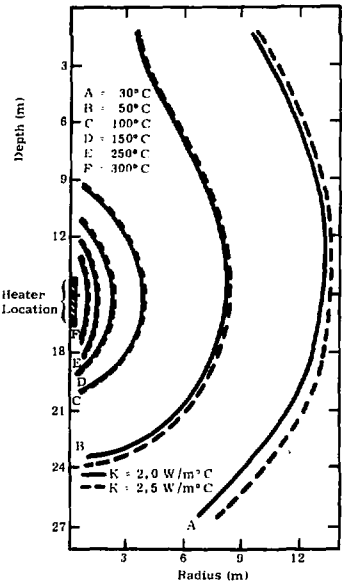

Figure 14. Calculated Isotherm Positions After 243 Days of Heater Operation, Using 2.0 and 2.5 W/m°C Thermal Conductivity and the Computer Code CINDA

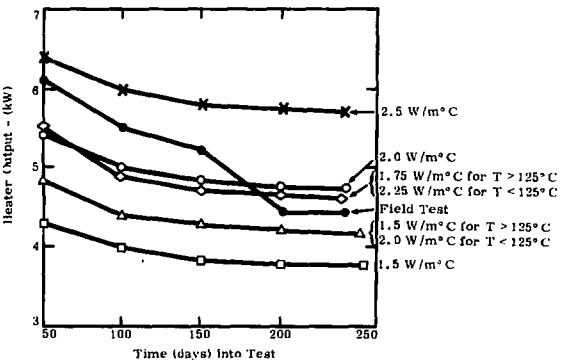

Figure 15. Comparison of Site 1 Heater Wattages Over Time With Wattages Predicted by CINDA From 50 to 240 Days

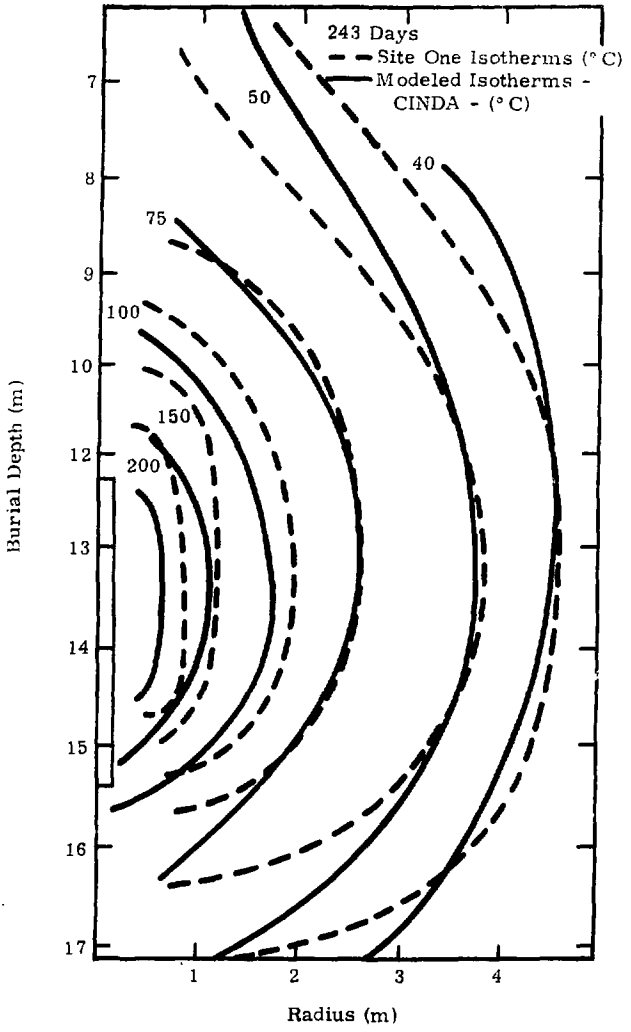

Figure 16. Comparison at 243 Days of Isotherms Measured at Site 1 and Those Calculated Using CINDA, Assuming Constant Thermal Conductivity of 2.0 W/m°C

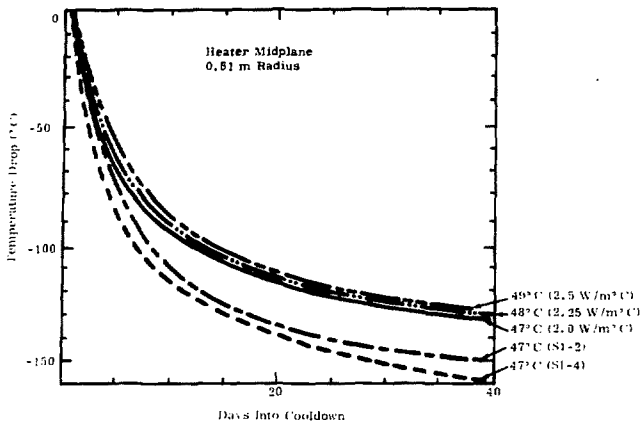

(a)

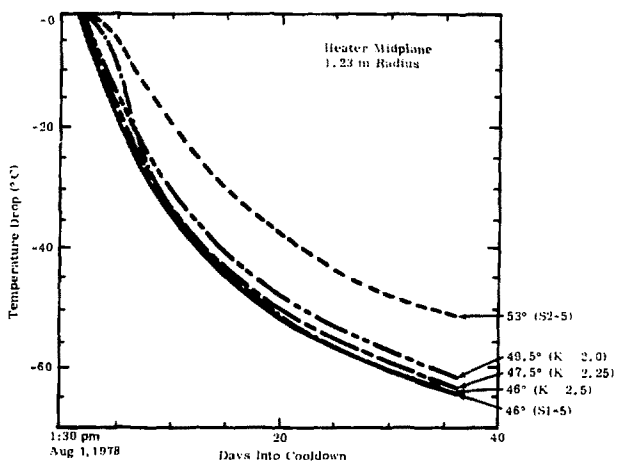

(b)

Figure 17. Comparison of Calculated (Upper Curve) and Actual (Lower Curve) Cooldown Rates in the Heater Midplane, Adjusted to Start at a Common Point. Final temperature together with modeled thermal conductivity or hole number are shown at the right.

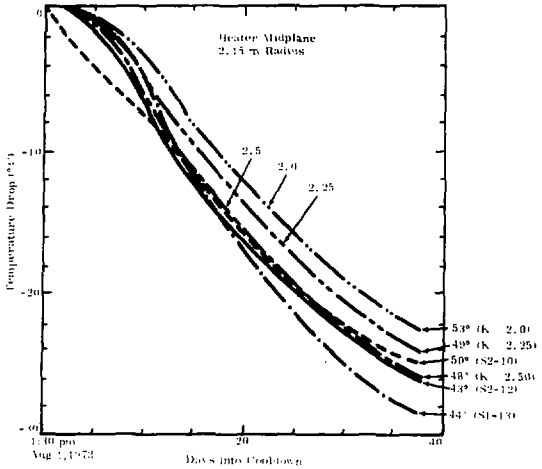

Figure 17. Continued

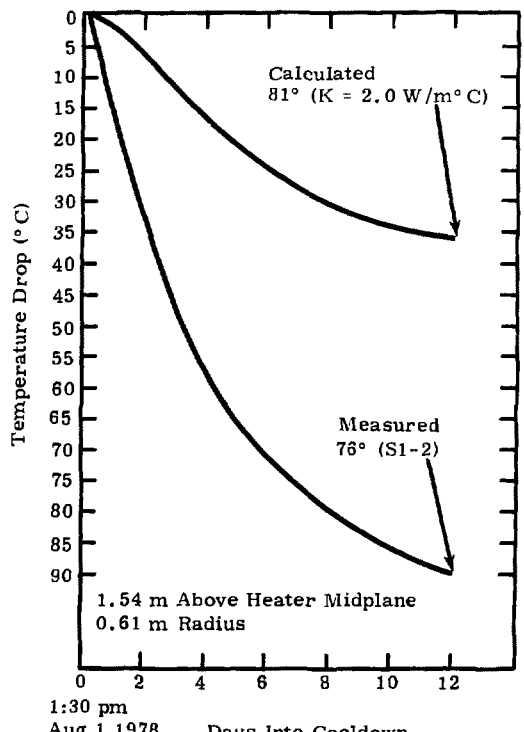

Figure 18. Comparison of Calculated and Actual Cooldown Rates at a Radius of 0.61 metre and 1.54 metre above the Heater Midplane. Final temperature together with modeled thermal conductivity or hole number are shown at the right.

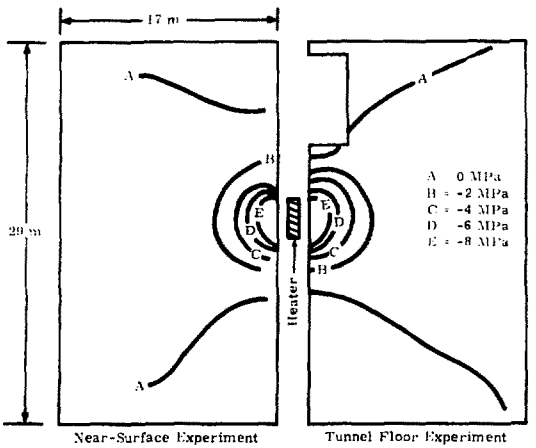

Figure 19. Calculated Radial Stress Distribution After 90 Days; Comparison of Near-Surface Test and At-Depth Floor Emplacement

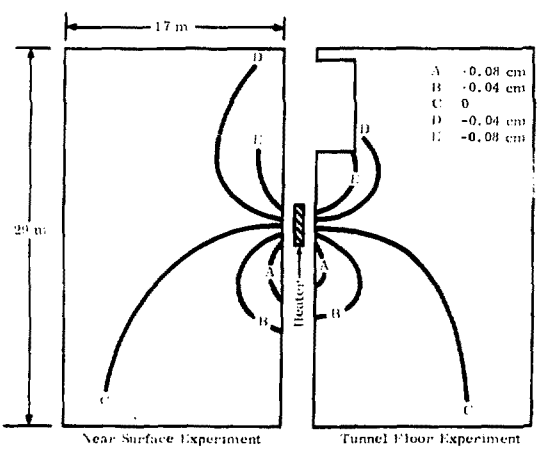

Figure 20. Calculated Vertical Displacements; Comparison of Near-Surface Test and At-Depth Floor Emplacement

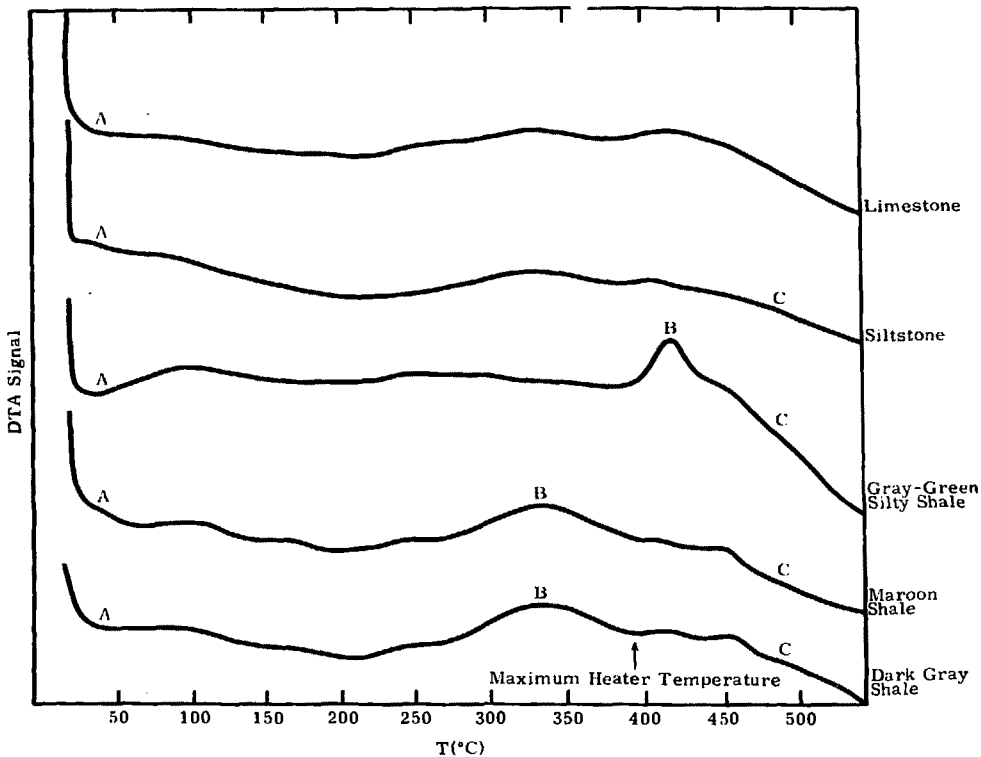

Figure 21. DTA Analyses of Various Conasauga Rock Types

Figure 22. Photomicrograph of Shale Showing Subparallel Alignment of Mineral Grains

Figure 73. Photomicrograph of Calcite-Silica Sill Rock Showing Orientation of Large Quartz Calcrete Mineral Grains

Figure 24. Photomicrograph of Interbedded Shale (Dark) and Limestone (Light) Offset by a Fracture Trending Obliquely to Bedding

Figure 25. A Relatively Rare Clean Break in Shale (Dark) That Subsequently Filled With Calcite (Light)

Figure 26. A More Typical Complex Fracture System in Shale

Figure 27. A Fossil Relic in Dark Gray Shale Unit

Figure 28. Heated Sample. Dark cluster is fine-grained iron pyrite. Note general reddish orange tint of sample and darker discoloration along open fracture due to iron oxidation. Maximum temperature experienced by sample was about 300°C

Figure 29. Silty Material Showing Preferential Oxidation on Fracture Surface. Maximum temperature experienced by sample was about 200°C.

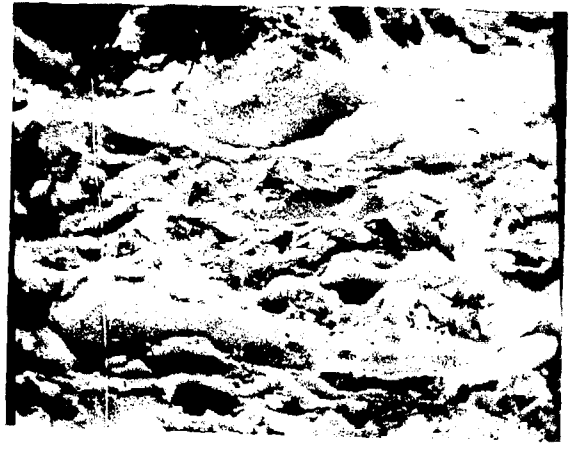

a. Before Heating

b. After (Max Temperature 200°C)

Figure 30. Scanning Electron Photomicrograph of Surfaces Broken Perpendicular to Bedding (666X)

a. Before Heating

b. After (Max Temperature 225°C)

Figure 31. Scanning Electron Photomicrograph of Bedding Surfaces (666X)

a. Before Heating

b. After (Max Temperature 175 C)

Figure 32. Scanning Electron Photomicrograph of Slickensided Fracture Surfaces (666X)

Figure 33. Gypsum Crystals That Formed After Cooling of the Site (200X)

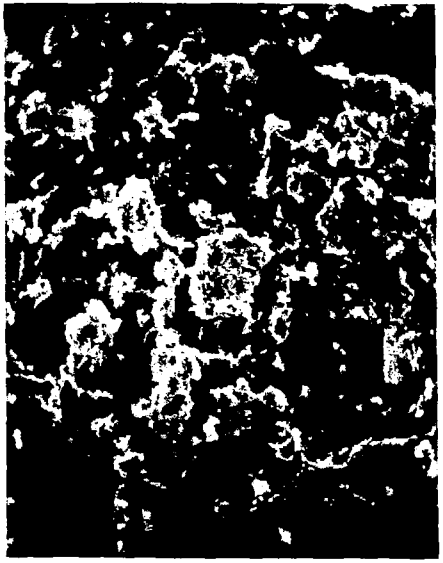

Figure 34. Scanning Electron Photomicrograph of a Fracture Surface at 200X

Figure 35. Scanning Electron Photomicrograph of the Same Fracture Surface at 2000X

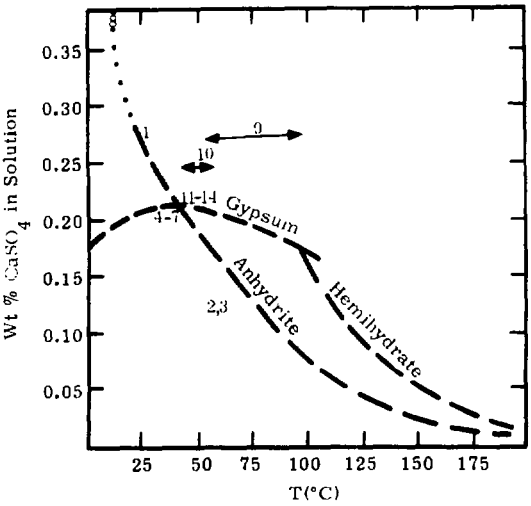

Figure 36. The Solubility of Anhydrite, Hemihydrate, and Gypsum in Water (Data plotted according to sample number in Table 3)

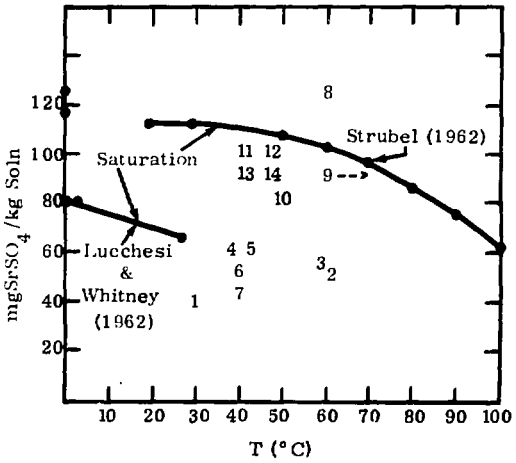

Figure 37. Strontium Sulfate Concentrations in Solution

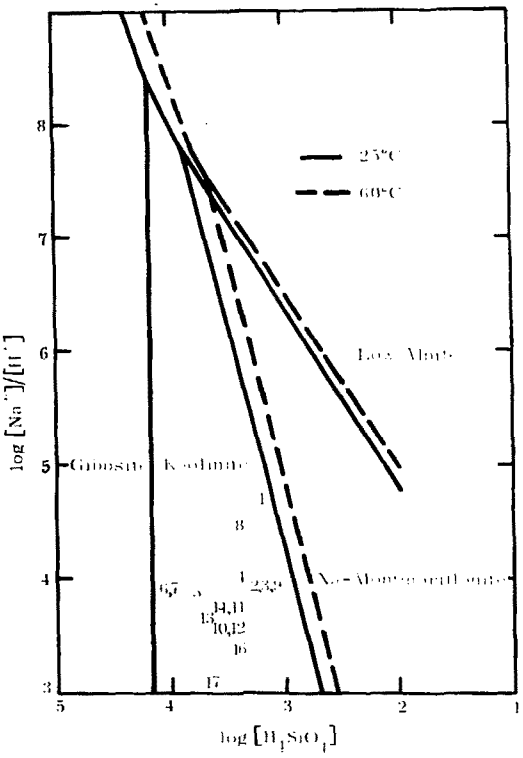

Figure 38. Solution Composition-Mineral Stability Relations in the System HCl--H_2O--Al_2O_3--Na_2O--SiO_2, at 25° and 60°C

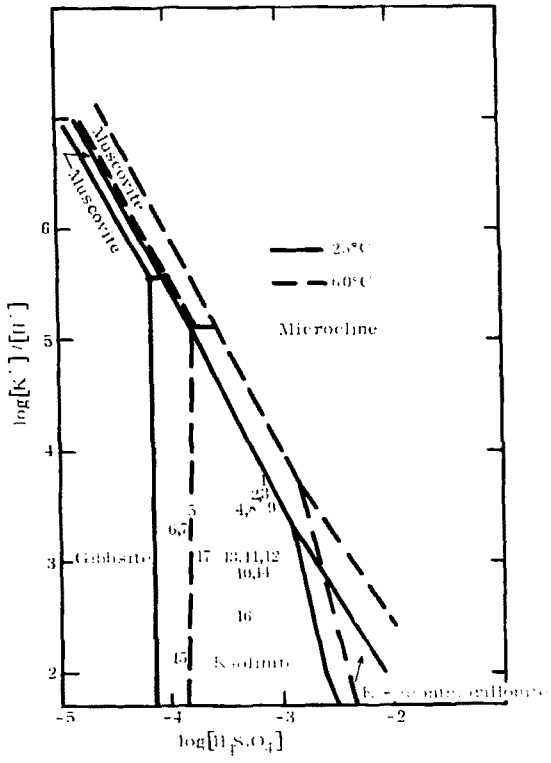

Figure 39. Solution Composition-Mineral Stability Relations in the System HCl--H_2O--Al_2O_3--K_2O--SiO_2, at 25° and 60°C

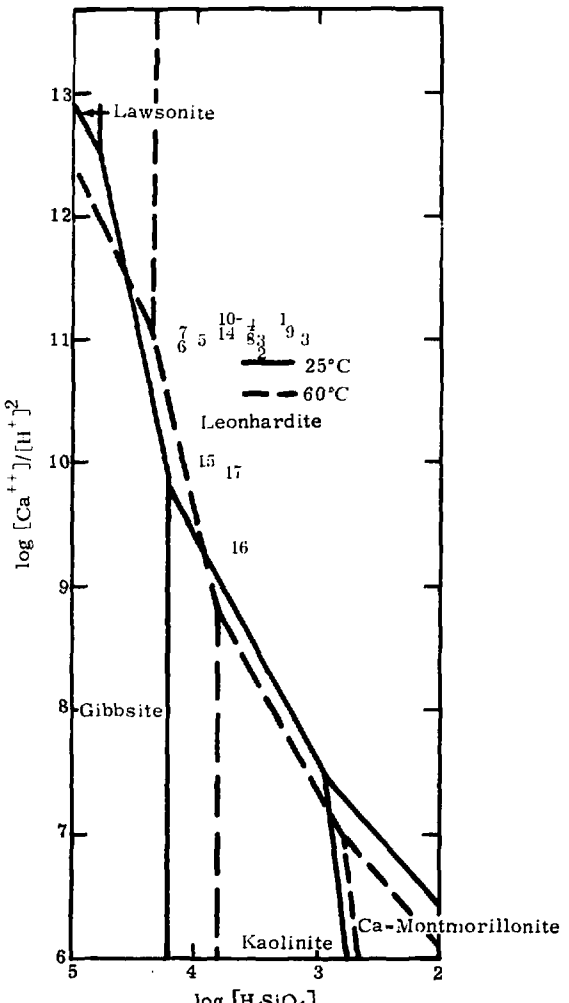

Figure 40. Solution Composition-Mineral Stability Relations in the System HCl--H_2O--Al_2O_3--CaO--CO_2--SiO_2, at 25° and 60°C

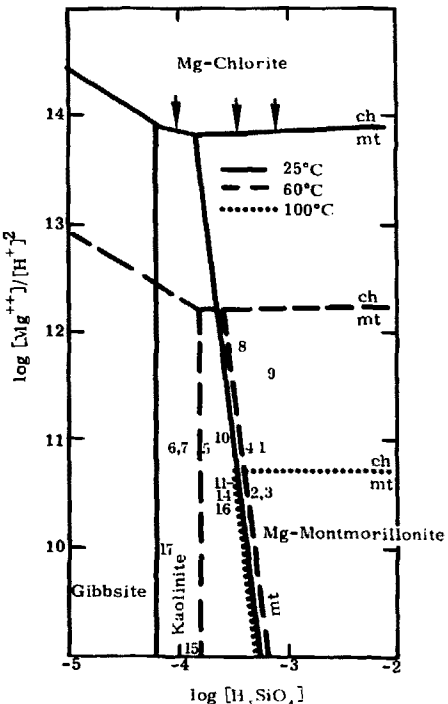

Figure 41. Solution Composition-Mineral Stability Relations in the System $HCl--H_2O--Al_2O_3--CO_2--MgO--SiO_2$, at 25°, 60°, and 100°C

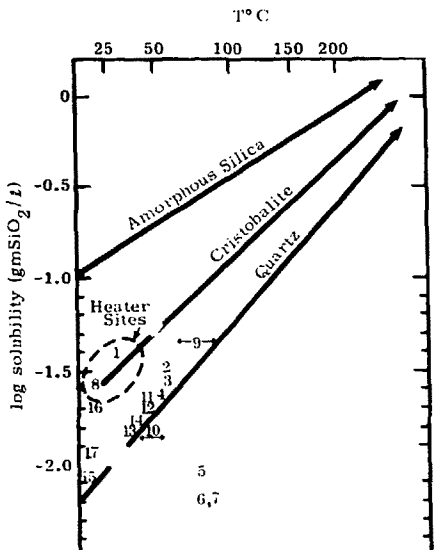

Figure 42. Solubility of Silica Polymorphs as a Function of Temperature

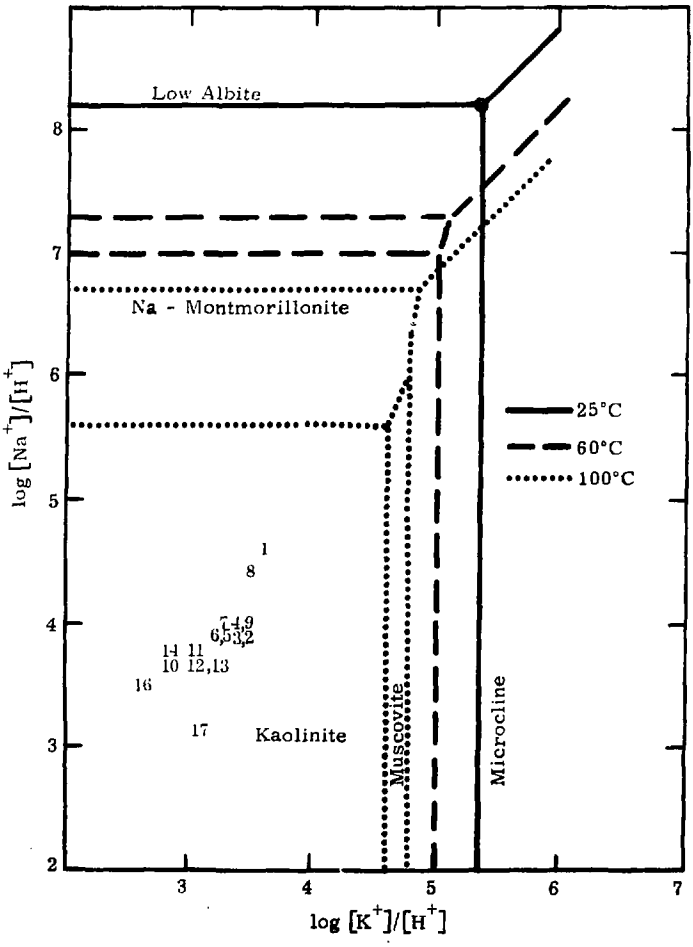

Figure 43. Solution Composition-Mineral Stability Relations in the System HCl--H_2O--Al_2O_3--K_2O--Na_2O--SiO_2, at 25°, 60°, and 100°C

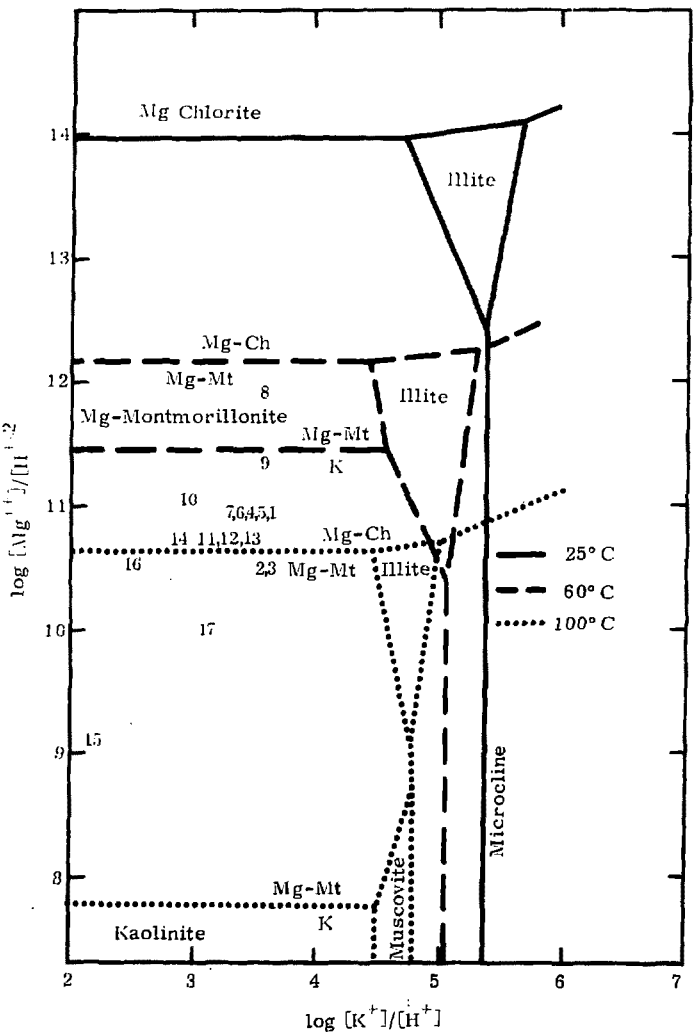

Figure 44. Solution Composition-Mineral Stability Relations in the System HCl--H_2O--Al_2O_3--K_2O--MgO--SiO_2 at 25°, 60°, and 100°C

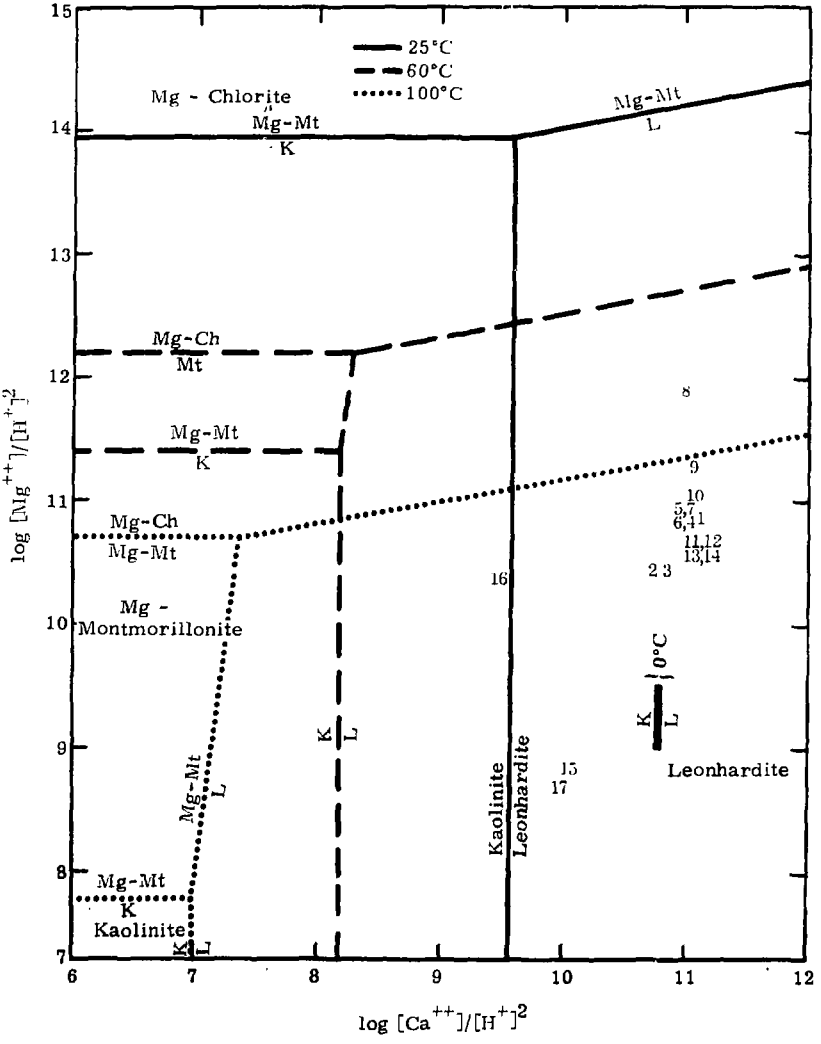

Figure 45. Solution Composition-Mineral Stability Relations in the System $HCl--H_2O--Al_2O_3--CaO--MgO--SiO_2$, at 25°, 60°, and 100°C

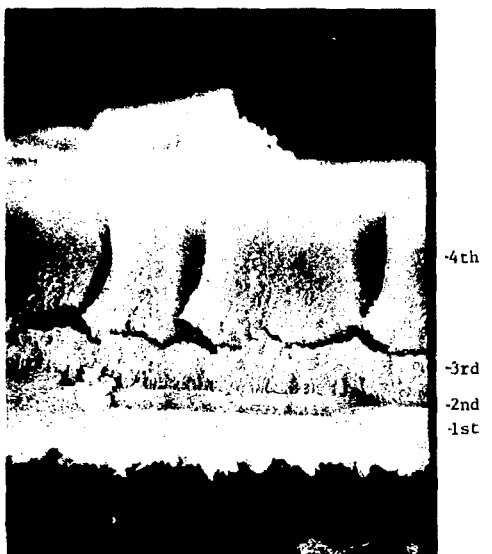

Figure 46. Scanning Electron Photomicrograph of an Edge View of the Alteration Layer, Outer Side Down

Figure 47. Scanning Electronic Photomiccograph of the Exterior of the Alteration Layer Showing a Mat of Acicular Crystals

Figure 48. Scanning Electron Photomicrograph of Glass Surface Beneath Gel Alteration Layer

Figure 49. Interior Surface of Gel Alteration Layer.

Figure 50. Corroded Thermocouples from Immediately Above the Site 1 Heater